Article

A Novel MOGNDO Algorithm for Security-Constrained Optimal Power Flow Problems

Sundaram B. Pandya [1], James Visumathi [2], Miroslav Mahdal [3,*], Tapan K. Mahanta [4] and Pradeep Jangir [5]

1 Department of Electrical Engineering, Shri K.J. Polytechnic, Bharuch 392 001, India
2 Department of Computer Science and Engineering, Vel Tech Rangarajan Dr Sangunthala R&D Institute of Science and Technology, Chennai 600 062, India
3 Department of Control Systems and Instrumentation, Faculty of Mechanical Engineering, VSB-Technical University of Ostrava, 17. Listopadu 2172/15, 708 00 Ostrava, Czech Republic
4 School of Mechanical Engineering, Vellore Institute of Technology, Chennai 600 127, India
5 Rajasthan Rajya Vidyut Prasaran Nigam, Losal, Sikar 332 025, India
* Correspondence: miroslav.mahdal@vsb.cz

Abstract: The current research investigates a new and unique Multi-Objective Generalized Normal Distribution Optimization (MOGNDO) algorithm for solving large-scale Optimal Power Flow (OPF) problems of complex power systems, including renewable energy sources and Flexible AC Transmission Systems (FACTS). A recently reported single-objective generalized normal distribution optimization algorithm is transformed into the MOGNDO algorithm using the nondominated sorting and crowding distancing mechanisms. The OPF problem gets even more challenging when sources of renewable energy are integrated into the grid system, which are unreliable and fluctuating. FACTS devices are also being used more frequently in contemporary power networks to assist in reducing network demand and congestion. In this study, a stochastic wind power source was used with different FACTS devices, including a static VAR compensator, a thyristor- driven series compensator, and a thyristor—driven phase shifter, together with an IEEE-30 bus system. Positions and ratings of the FACTS devices can be intended to reduce the system's overall fuel cost. Weibull probability density curves were used to highlight the stochastic character of the wind energy source. The best compromise solutions were obtained using a fuzzy decision-making approach. The results obtained on a modified IEEE-30 bus system were compared with other well-known optimization algorithms, and the obtained results proved that MOGNDO has improved convergence, diversity, and spread behavior across PFs.

Keywords: FACTS controller; MO-OPF; meta-heuristics; probability density function; stochastic; WTGS

1. Introduction

Constraint-based optimization problems with multiple objectives are the most prevalent type. In contrast to single-objective optimization problems, multi-objective optimization problems have a wide variety of optimal solutions. The PF is an assortment of perfect responses [1,2]. A multi-objective optimization approach must be able to locate solutions that are uniform in the generated PFs and are workable optimum solutions to address multi-objective problems [3]. Multi-objective optimization approaches are challenged by the simultaneous achievement of these many objectives [4]. MH algorithms are typically tested on simpler, well-known optimization scenarios. However, unlike classic search problems, engineering design tasks can have different specifications. Modifying and developing the algorithm for them is the most effective way to optimize for them. The realm of application of multi-objective optimization algorithms is quite vast, ranging from machining processes [5,6], to vehicle routing [7], to optimizing AI systems [8].

Power systems researchers have been seeking solutions to the OPF challenges for many decades. One issue with managing power systems and making plans for modern electrical

energy networks is working with systems that use non-conventional sources of energy. Ullah et al. [9] developed a hybrid phasor particle swarm optimization and gravitational search algorithm to address the OPF problem in the wind and solar energy systems that are connected to electrical power grids, while accounting for the control variables (PPSOGSA). For the OPF problem with wind and solar systems, the developed PPSOGSA algorithm produced outstanding and helpful results. In Elattar's research, the OPF problem was principally modelled mathematically using a combined heat and power system with stochastic wind energy. On an IEEE 30-bus test system under various test situations, the suggested method was assessed. The formulation of the OPF problem covering energy sources and the suggested approach to solve it produced effective answers in contrast to pre-existing algorithms [10] that were used to address similar problems. Anongpun et al. [11] used IEEE 30- and 118-bus test systems to study the use of enhanced particle swarm optimization (PSO) to solve a multi-objective OPF problem using a wind energy system that combined chaotic mutation and stochastic weights. When compared to the other algorithms included in their study, the suggested method produced better results. Salkuti [12] used the glowworm swarm optimization method to offer a solution to a multi-objective OPF problem requiring a modern electrical energy system that utilized wind energy. On IEEE 30- and 300-bus test systems, the methodology was examined in many operational scenarios. The simulation findings indicated that the proposed methodology might offer an alternative. A flower pollination algorithm was used by Kathiravan et al. [13] to address the OPF problem using coal-based, wind, and solar energy systems. In a variety of test situations, the authors used their method to test systems for the IEEE 30-bus and Indian utility 30-bus. Duman et al. [14] used differential evolutionary particle swarm optimization to address the OPF problem (DEEPSO) with manageable wind and solar (PV) energy sources. IEEE 30-, 57-, and 118-bus test systems were used to evaluate the DEEPSO technique to explore the issue under various objective functions. DEEPSO produced better simulation results when compared to the other optimization approaches that were looked at [14]. They recommended using FACTS devices such as a thyristor-controlled phase shifter (TCPS) and a thyristor-controlled series capacitor (TCSC) to solve the OPF problem. To account for the uncertainties associated with wind energy installation, they used chaotic maps and a modified version of the PSOGSA (particle swarm optimization and gravitational search algorithm). The method presented [15] appears to be a potential approach for a solution based on the findings of simulations. Biswas et al. [16] solved the OPF challenge, which incorporated coal-based, wind, solar, and small-hydro energy sources coupled to IEEE 30-bus test systems, by running multiple rounds of the multi-objective evolutionary algorithm. The constrained multi-objective population extremal optimization (CMOPEO) technique was used to handle the wind and solar-integrated OPF problem by Chen et al. [17], who also tested the method on an IEEE 30-bus for different scenarios. Additionally, research has been done on the evolutionary particle swarm optimization (EPSO) [18], the hybrid differential evolution and symbiotic organisms search algorithm (HMICA-SQP) [19], the success-history-based adaptation of differential evolution with superiority of feasible solutions (SHADE-SF) [20], and the hybrid modified imperialist competitive algorithm and sequential quadratic programming algorithm (HMICA-SQP) [21]. Pandya and Jariwala [22] addressed single and multi-objective OPF issues by integrating with various sustainable energy sources using recently developed metaheuristics algorithms. Biswas et al. [23] analyzed the integration of three FACTS devices, wind turbines, and coal-fired power plants. The success history-based adaptive differential evolution (SHADE) method was used to conduct the investigation. According to the "No Free Lunch (NFL)" theorem [24], no metaheuristic can solve every issue that occurs in real-world situations. This theorem has opened the door to the creation of both novel metaheuristic techniques and improvements to existing ones.

When using the Generalized Normal Distribution Optimization method [25] in multi-objective optimization scenarios, several things need to be taken into account. The initial problem in multi-objective generalized normal distribution optimization is balancing con-

vergence and divergence archives. The algorithm's generated solution set is filtered according to a certain quality metric, and the non-dominating solution set is kept in separate, external archives. In the literature, there are numerous recommendations for constructing archives that could be employed in the multi-objective Generalized Normal Distribution Optimization method. The pre-defined maximum size archives are widely employed, since more non-dominating solutions can emerge quickly. The algorithm's ability to begin with the straightforward determination of the required population size and the terminal condition is the most noticeable feature of the GNDO. The location of the person is automatically changed by the generalized normal distribution function (GNDO), which has a simple construction. The benefits and drawbacks of the GNDO algorithm are as follows:

- It offers a faster and smoother convergence, especially for difficult problems, and it strikes the perfect balance between exploration and exploitation.
- Local minima are less likely to become entangled in relaxed convergence.
- Effortlessly simple, adaptable, and simple to use
- The traditional GNDO may have issues with convergence trends or become stuck in narrow, deceptive optima for challenging optimization tasks, such as high-dimensional and multimodal problems.

Currently, both conventional and non-conventional energy sources require more studies. The current body of research recommends using coal-based plus wind and FACTS devices, combined with single and multi-objective optimum power flow (MOOPF) problems. The conventional IEEE 30-bus network has been altered to include non-conventional sources for research purposes. Using Weibull PDF, non-conventional units' stochastic behaviors are calculated. The generating cost is suitably adjusted to account for reserve cost if these stochastic units are over-estimated and adjusted for penalty cost in the case that they are underestimated. Using the Generalized Normal Distribution Optimization method, Pareto solution clusters are discovered for the multi-objective problem. The following is a list of the contributions made by this study:

1. This work focuses on the mathematical modelling of the single and multiple-objective OPF issue modelled, which takes into account both conventional units and non-conventional sources of energy units, as well as FACTS devices.
2. The appropriate probability density functions (PDFs) are modeled in the second stage to describe the wind power plants' random behavior.
3. Stochastic non-conventional sources of energy sources are among the single and multiple-objective OPF issues for which the Non-Dominated Sorting Generalized Normal Distribution Optimization (NSGNDO) technique is used to develop solutions.
4. Studies and performance evaluations of the MOGNDO algorithm using empirical comparisons are conducted.

The notion of the mathematical models for coal-based power, wind power, and FACTS devices is presented in Section 2 of the study. An explanation of the objectives that need to be optimized is included in Section 3. Section 4 provides an explanation and illustrations of the multi-objective GNDO technique. Section 5 presents numerical results and discussion, and Section 6 provides concluding remarks.

2. Mathematical Representations

The case studies presented here restructure the original IEEE 30-bus test apparatus. The modified approach incorporates wind turbines and FACTS devices, and is listed in Table 1. The equipment used for the analysis is depicted in Figure 1. The placement and ratings of FACTS devices are depicted in the diagram with dotted lines because they have been optimized. The section below provides information on the costs of traditional coal-based production facilities and plants using non-conventional sources of energy.

Table 1. Test system key features for analysis.

Particulars	Quantity	Details
Total buses	30	[23]
Total branches	41	[23]
Coal-based generators (TG1; TG2; TG3; TG4)	4	Buses: 1 (swing), 2, 8 and 13
Wind generators (WG1; WG2)	2	Bus-5 and Bus-11
Tap changing transformers	4	Branches: 11, 12, 15 and 36
SVC	2	Optimal bus and rating derived
TCSC	2	Optimal branch position and rating derived
TCPS	2	Optimal placement and rating derived
Demand	-	283.4 MW, 126.2 MVAr
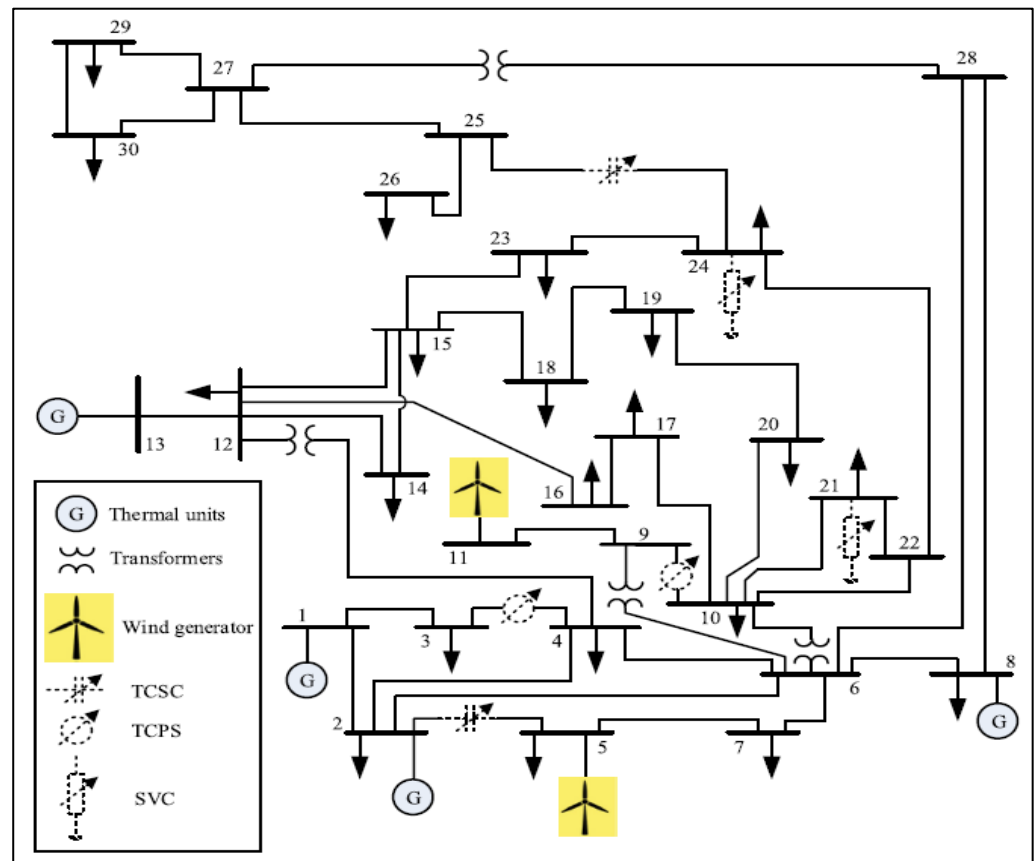
Figure 1. Adapted IEEE 30-bus scheme with power units and FACTS policies [23].

2.1. Cost of Coal-Based Power Units

The generalized quadratic equation for the calculation of generation cost is expressed in (1) in $/h [23]:

$$C_{T0}(P_{TG}) = \sum_{i=1}^{N_{TG}} a_i + b_i P_{TGi} + c_i P_{TGi}^2 \tag{1}$$

For a more practical case, the valve point effect included:

$$C_T(P_{TG}) = \sum_{i=1}^{N_{TG}} a_i + b_i P_{TGi} + c_i P_{TGi}^2 + \left| d_i \times \sin\left(e_i \times \left(P_{TGi}^{min} - P_{TGi}\right)\right) \right| \tag{2}$$

The values of both coal-based price constants and emanation constants with various scenarios are shown in [23].

2.2. Toxic Gas Emanation

Polluted gases are released by using coal-based plants. So, toxic gas emanations in tons per hour can be determined as (in ton/h):

$$F2 = \mathrm{t}, E = \sum_{i=1}^{N_{TG}} \left[\left(\alpha_i + \beta_i P_{TGi} + \gamma_i P_{TGi}^2 \right) \times 0.01 + \omega_i e^{(\mu_i P_{TGi})} \right] \tag{3}$$

The toxic gas emanation constants of coal-based power plants are taken from [22].

2.3. Direct Cost of Stochastic Non-Conventional Sources Plants

It is particularly challenging to integrate non-conventional energy sources into the power grid since they are stochastic. The independent system operator (ISO) is responsible for managing these non-conventional energy sources. Due to this, the private operator must contract with the grid or ISO for a specific quantity of planned power. The scheduled electricity must be maintained by the ISO scheduled power. If these non-conventional sources are unable to maintain the planned power, the ISO is liable for the absence of power. So, if a need arises, there are spinning reserve requirements. This spinning reserve increases costs for the ISO, and this circumstance is known as an overestimation of non-conventional sources. Conversely, if non-conventional sources formed more energy than was planned, it might go to waste, due to underuse. Therefore, the ISO must accept the penalty charge. The scheduled power cost, the overestimation cost caused by the spinning reserve, and the penalized cost caused by the underestimation are the three costs related to electricity. The direct cost linked to wind farms is demonstrated with the P_{ws} scheduled power from the same sources as:

$$C_w(P_{ws}) = g_w P_{ws} \tag{4}$$

2.4. Indeterminate Non-Conventional Sources of Wind Power Cost

Due to the erratic nature of wind, the wind farm occasionally produces less energy than expected. This means that if demand increases, it needs the spinning reserve to maintain the agreed-upon amount of scheduled power. It is sometimes feasible that the real power generated by wind farms won't be enough to meet demand and will have lower values. Such power is referred to as exaggerated power by an ambiguous resource. To control this kind of uncertainty and provide end users with a reliable power source, the network ISO operates spinning reserves. The price of hiring a backup generator to supply the overestimated power is known as the reserve cost.

Reserve cost for the wind unit is formulated by:

$$C_{Rw}(P_{ws} - P_{wav}) = K_{Rw}(P_{ws} - P_{wav}) = K_{Rw} \int_0^{P_{ws}} (P_{ws} - p_w) f_w(p_w) dp_w \tag{5}$$

The possibility exists that the wind farm will generate more power than is required, which is the opposite of the overestimation scenario. Underestimated power is the term used to describe such a situation. If there is no provision for managing the output power from coal-based units, the excess power will be lost. Regarding the extra power, the ISO needs to be penalized.

The penalty charge for the wind unit is given by:

$$C_{Pw}(P_{wav} - P_{ws}) = K_{Pw}(P_{wav} - P_{ws}) = K_{Pw} \int_{P_{ws}}^{P_{wr}} (p_w - P_{ws}) f_w(p_w) dp_w \tag{6}$$

2.5. Uncertainty Models of Stochastic Wind Units

In the redesigned IEEE-30, the wind power generating units installed at buses 5 and 11, which were originally thermal generators, were replaced. It should be noted that, as for a comparison point of view with the published reference article [23], in this paper, the thermal DGs were also replaced with the wind turbines. This will ensure compatibility of the results obtained by the proposed algorithm to the already published research article [23]. The scale (*c*) and shape (*k*) constants for the proposed Weibull model are detailed in Table 2.

Table 2. PDF constants of wind power plants [23].

Windfarm	No. of Turbines	Rated Power	Weibull PDF Parameters	Cost Constants		
				Direct	Reserve	Penalty
WG5 (bus 5)	25	75	$c = 9, k = 2$	1.60	3.0	1.50
WG11 (bus 11)	20	60	$c = 10, k = 2$	1.75	3.0	1.50

The Weibull curve and wind frequency distributions in Figure 2 (for the bus 5 wind plant) and Figure 3 (for the bus 11 wind plant) were produced using 8000 Monte-Carlo settings. The standard provided explains the need for wind turbine design and specifies the maximum turbulence class IA that is confirmed to operate at the highest yearly average wind velocity of 10 m/s at hub height. The formed shape (k) and scale (c) parameters of wind farms are given particular attention, because their highest Weibull mean value is fixed at around 10. It is commonly known that the wind speed distribution follows the Weibull PDF curve.
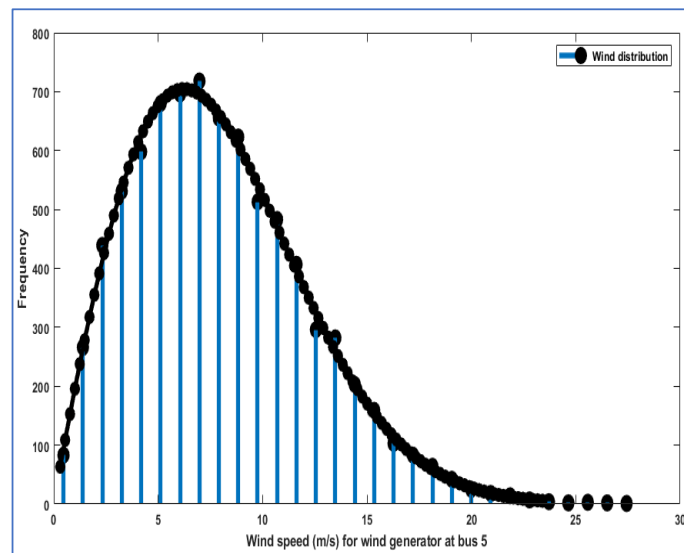

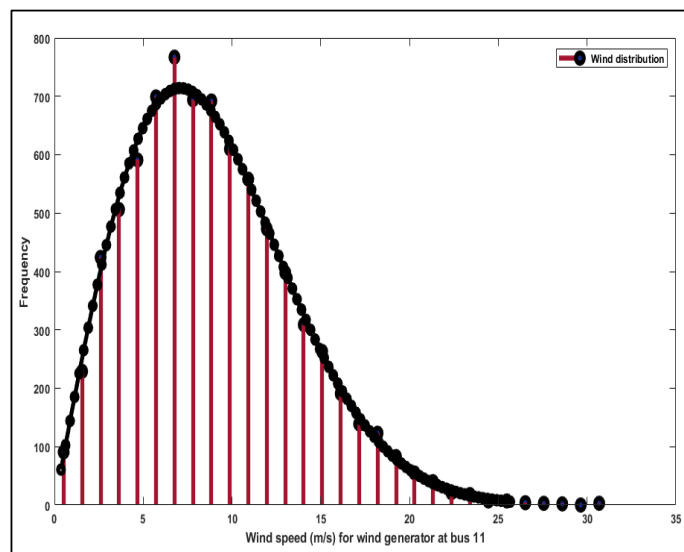**Figure 2.** Weibull PDF (bus 5).

Figure 3. Weibull PDF (bus 11).

The following formula can be used to calculate the probability of wind velocity v, in m/s, pursuing the Weibull PDF with shape factor (k) and scale factor (c) [23]:

$$f_v(v) = \left(\frac{k}{c}\right)\left(\frac{v}{c}\right)^{(k-1)} e^{-\left(\frac{v}{c}\right)^k} \, for \;\; 0 < v < \infty \tag{7}$$

The Weibull distribution's mean is given as follows [23]:

$$M_{wbl} = c * \Gamma\left(1 + k^{-1}\right) \tag{8}$$

and the gamma function $\Gamma(x)$ is expressed in Equation (9):

$$\Gamma(x) = \int_0^\infty e^{-t} t^{x-1} dt \tag{9}$$

2.6. Average Power Calculation for Wind Plants

The combined outputs of the 25 turbines in the farm are taken as the wind unit connected at bus 5. Every turbine has a 3 MW output rating. The wind velocity affects the wind turbine's precise output, which varies. We used the following equations to express turbine output power in terms of wind velocity (v) [23]:

$$p_w(v) = \begin{cases} 0, & \text{for } v \langle v_{in} \text{ and } v \rangle v_{out} \\ p_{wr}\left(\frac{v - v_{in}}{v_r - v_{in}}\right) & \text{for } v_{in} \leq v \leq v_r \\ p_{wr} & \text{for } v_r < v \leq v_{out} \end{cases} \tag{10}$$

The Enercon E82-E4 design specification is referred to for the 3 MW wind turbine. The various speeds are v_{in} = 3 m/s, v_r = 16 m/s, and v_{out} = 25 m/s.

2.7. Wind Power Probabilities Calculation

In certain ranges of wind speeds, uncertain wind generation is noticeable. The generated power would be 0 if the wind speed was greater than or less than the cut-out speed or cut-in speed. The turbine thereby produces the specified amount of power within the range of the rated and cut-out wind speeds. These are possible ways to describe the likelihood of these areas [23]:

$$f_w(p_w)\{p_w = 0\} = 1 - \exp\left[-\left(\frac{v_{in}}{c}\right)^k\right] + \exp\left[-\left(\frac{v_{out}}{c}\right)^k\right] \tag{11}$$

$$f_w(p_w)\{p_w = p_{wr}\} = \exp\left[-\left(\frac{v_r}{c}\right)^k\right] - \exp\left[-\left(\frac{v_{out}}{c}\right)^k\right] \tag{12}$$

Between the cut-in velocity and the rated velocity of the wind, the wind production remains constant. The following can be used to express the likelihood of the continuous zone [23]:

$$f_w(p_w) = \frac{\beta(v_r - v_{in})}{\alpha^\beta * p_{wr}} \left[v_{in} + \frac{p_w}{p_{wr}}(v_r - v_{in})\right]^{\beta-1} \exp\left[-\left(\frac{v_{in} + \frac{p_w}{p_{wr}}(v_r - v_{in})}{\alpha}\right)^\beta\right] \tag{13}$$

2.8. Thyristor-Controlled Series Compensator (TCSC) Modeling

The basic circuitry of the TCSC is depicted in Figure 4. It consists of a fixed series capacitor (XC) and a reactor (XL) operated by a thyristor. For the TCSC to function as a variable capacitive reactance, reactance $X_C < X_L$ is taken into consideration. By varying the firing angle (α) of the thyristors, the inductive reactance is changed, and for high values of inductive reactance, the least corresponding capacitive reactance is produced (Open circuit

Inductive branch). As a result, the TCSC's effective reactance with constant capacitive reactance X_C and variable inductive reactance $X_L(\alpha)$ can be written as [23]:

$$X_{TCSC}(\alpha) = \frac{X_C X_L(\alpha)}{X_L(\alpha) - X_C} = -jX_C \tag{14}$$
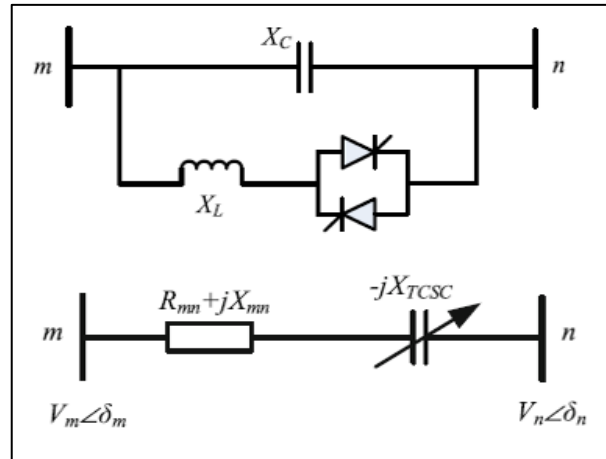
Figure 4. Basic Structure and model of TCSC [23].

The TCSC static model, which is situated in the path between buses m and n, is shown in Figure 4. Following the TCSC's integration (described as a variable capacitive reactance mode), the transmission line's adjusted reactance (X_{eq}) is given by [23]:

$$X_{eq} = X_{mn} - X_{TCSC} = (1 - \tau)X_{mn} \tag{15}$$

where

$$\tau = \frac{X_{TCSC}}{X_{mn}} \tag{16}$$

The power flow equations of the line incorporating the TCSC are written as [23]:

$$\begin{aligned} P_{mn} = V_m^2 g_{mn} - V_m V_n g_{mn} \cos(\delta_m - \delta_n). \\ -V_m V_n b_{mn} \sin(\delta_m - \delta_n) \end{aligned} \tag{17}$$

$$\begin{aligned} Q_{mn} = -V_m^2 b_{mn} - V_m V_n g_{mn} \sin(\delta_m - \delta_n). \\ +V_m V_n b_{mn} \cos(\delta_m - \delta_n) \end{aligned} \tag{18}$$

$$\begin{aligned} P_{nm} = V_n^2 g_{mn} - V_m V_n g_{mn} \cos(\delta_m - \delta_n). \\ +V_m V_n b_{mn} \sin(\delta_m - \delta_n) \end{aligned} \tag{19}$$

$$\begin{aligned} Q_{nm} = -V_n^2 b_{mn} + V_m V_n g_{mn} \sin(\delta_m - \delta_n). \\ +V_m V_n b_{mn} \cos(\delta_m - \delta_n) \end{aligned} \tag{20}$$

where

$$g_{mn} = \frac{r_{mn}}{r_{mn}^2 + (x_{mn} - x_c)^2} \tag{21}$$

$$b_{mn} = -\frac{x_{mn} - x_c}{r_{mn}^2 + (x_{mn} - x_c)^2} \tag{22}$$

2.9. Model of Thyristor-Controlled Phase Shifter (TCPS)

Figure 5 displays the model of the TCPS placed between the line that connects buses m and n. The power flow equations of the line can be expressed as below, assuming that is the phase shift angle ϕ is introduced by the TCPS:

$$P_{mn} = \frac{V_m^2 g_{mn}}{\cos^2 \phi} - \frac{V_m V_n}{\cos \phi}[g_{mn}\cos(\delta_m - \delta_n + \phi). \\ +b_{mn}\sin(\delta_m - \delta_n + \phi)] \tag{23}$$

$$Q_{mn} = -\frac{V_m^2 b_{mn}}{\cos^2 \phi} - \frac{V_m V_n}{\cos \phi}[g_{mn}\sin(\delta_m - \delta_n + \phi). \\ -b_{mn}\cos(\delta_m - \delta_n + \phi)] \tag{24}$$

$$P_{nm} = V_n^2 g_{mn} - \frac{V_m V_n}{\cos \phi}[g_{mn}\cos(\delta_m - \delta_n + \phi). \\ -b_{mn}\sin(\delta_m - \delta_n + \varphi)] \tag{25}$$

$$Q_{nm} = -V_n^2 b_{mn} + \frac{V_m V_n}{\cos \phi}[g_{mn}\sin(\delta_m - \delta_n + \phi). \\ +b_{mn}\cos(\delta_m - \delta_n + \varphi)] \tag{26}$$
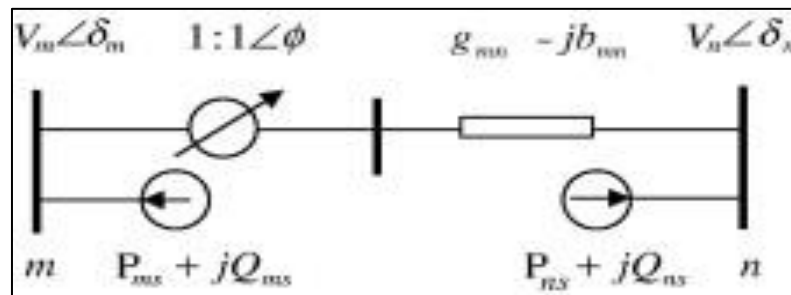
Figure 5. Model of TCP [23].

The inserted actual and reactive power of the TCPS at bus m and n is [23]:

$$P_{ms} = -g_{mn}V_m^2\tan^2\phi - V_m V_n\tan\phi[g_{mn}\sin(\delta_m - \delta_n). \\ -b_{mn}\cos(\delta_m - \delta_n)] \tag{27}$$

$$Q_{ms} = b_{mn}V_m^2\tan^2\phi + V_m V_n\tan\phi[g_{mn}\cos(\delta_m - \delta_n). \\ +b_{mn}\sin(\delta_m - \delta_n)] \tag{28}$$

$$P_{ns} = -V_m V_n\tan\phi[g_{mn}\sin(\delta_m - \delta_n) + b_{mn}\cos(\delta_m - \delta_n)] \tag{29}$$

$$Q_{ns} = -V_m V_n\tan\phi[g_{mn}\cos(\delta_m - \delta_n) - b_{mn}\sin(\delta_m - \delta_n)] \tag{30}$$

2.10. Model of Static VAR Compensator (SVC)

The basic circuit architecture and the SVC model are depicted in Figure 6. It is made up of a thyristor-controlled reactor ($X_L = \omega L$) and a fixed capacitor ($X_C = 1/\omega C$). By changing the thyristor firing angle (α), the reactance can be changed. The equivalent susceptibility is computed as:

$$B_{eq} = B_L(\alpha) + B_C \tag{31}$$

where

$$B_L(\alpha) = -\frac{1}{\omega L}\left(1 - \frac{2\alpha}{\pi}\right), B_c = \omega \times C \tag{32}$$

The reactive power offered by the SVC can be expressed in terms within the context of power flow:

$$Q_{SVC} = -V_m^2 \cdot B_{SVC} \tag{33}$$
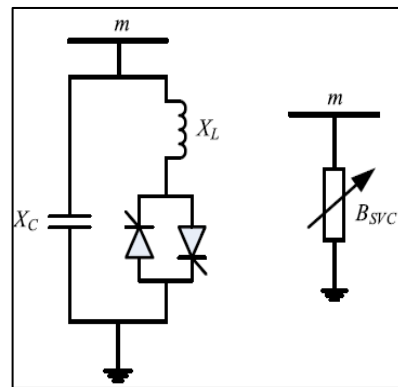
Figure 6. Basic structure and model of SVC [23].

3. Objectives of Optimization

The best active power allocation and the best VAR power allocation are goals in the OPF. The following are some examples of how this section incorporates the goals of wind power flow optimization.

3.1. Reducing Overall Costs While Using Non-Conventional Energy Sources

Objective 1:

Minimizing the whole cost is the first goal. Direct, reserve, and penalty charges for non-conventional resources are added to the coal-based unit cost to determine the overall generation cost. Therefore, the comprehensive cost for coal-based and wind power plants is denoted as:

Minimize—

$$F1 = C_{Tot} = C_T(P_{TG}) + [C_w(P_{ws}) + C_{Rw}(P_{ws} - P_{wav}) + C_{Pw}(P_{wav} - P_{ws})] \tag{34}$$

3.2. Reduction of Voltage Variation with the Use of Non-Conventional Energy Sources

One of the most crucial safety and administrative superiority lists is the bus voltage. By restricting the voltage deviations of the PQ bus from 1.0 for each unit, the improving voltage profile will be acquired. The objective function is going to come from:

Objective 2: Minimize—

$$F2 = \sum_{i=1}^{N_{pq}} |v_i - 1.0| \tag{35}$$

3.3. Minimization of APL Including Non-Conventional Energy Sources

The optimization of actual power losses P_{LOSS} (MW) maybe calculated by:

Objective 3: Minimize—

$$F3 = P_{LOSS} = \sum_{i=1}^{NB} P_{Gi} - \sum_{i=1}^{NB} P_{Di} \tag{36}$$

3.4. Enhancement of VSI Including Non-Conventional Energy Sources

The L_{max} index is the most important indicator for evaluating each bus's voltage constancy margin, since it keeps the voltage constant within a reasonable range during typical operation. For every PQ bus, the L_{max} index offers a scalar number. Between '0' (no load) and '1' is where the L_{max} index is located (voltage collapse). The following formula is used to get the *j*th bus's voltage collapse indicator amount:

$$L_j = \left| 1 - \sum_{i=1}^{N_g} F_{ji} \frac{V_i}{V_j} \right| \quad \forall j = 1, 2, \ldots \ldots, NL \tag{37}$$

$$F_{ji} = -[Y_1]^{-1}[Y_2] \tag{38}$$

The objective function of voltage stability enhancement is written by:

$$F4 = L = \max\left(L_j\right) \quad \forall j = 1, 2, \ldots\ldots, NL \tag{39}$$

3.5. Minimization of Entire Gross Cost Including Non-Conventional Energy Resources

The generating cost is significantly higher in the latter scenario, whereas the loss is greater in the former, as shown by Objectives 1 and 3. The requirement for an aim that includes both the cost and the loss is increased by this very circumstance. Making a cost model that converts the loss into an equivalent energy cost is a straightforward way to take into consideration both goals. The price of energy taken into account in this analysis is $0.10 per kWh. The goal of gross cost in dollars per hour might be stated as follows:

$$F5 = C_{Tot} + P_{LOSS} * 10000 * 0.10 \tag{40}$$

3.6. Equality Constraints

Power flow equations provide equality boundaries, and demonstrate that both real and fictitious power generated in a system should fulfill the load demand and system losses:

$$P_{Gi} - P_{Di} - V_i \sum_{j=1}^{NB} V_j \left[G_{ij} \cos\left(\delta_{ij}\right) + B_{ij} \sin\left(\delta_{ij}\right) \right] = 0 \quad \forall i \in NB \tag{41}$$

$$Q_{Gi} - Q_{Di} - V_i \sum_{j=1}^{NB} V_j \left[G_{ij} \sin\left(\delta_{ij}\right) - B_{ij} \cos\left(\delta_{ij}\right) \right] = 0 \quad \forall i \in NB \tag{42}$$

3.7. Inequality Constraints

Inequality bounds are the operational boundaries of devices and the security bounds of lines and PQ buses.

Generator bounds:

$$P_{TGi}^{min} \leq P_{TGi} \leq P_{TGi}^{max} \, \forall i \in N_{TG} \tag{43}$$

$$P_{ws}^{min} \leq P_{ws} \leq P_{ws}^{max} \tag{44}$$

$$Q_{TGi}^{min} \leq Q_{TGi} \leq Q_{TGi}^{max} \, \forall i \in N_{TG} \tag{45}$$

$$Q_{ws}^{min} \leq Q_{ws} \leq Q_{ws}^{max} \tag{46}$$

$$V_{Gi}^{min} \leq V_{Gi} \leq V_{Gi}^{max}, i = 1, \ldots\ldots, NG \tag{47}$$

Security bounds:

$$V_{L_p}^{min} \leq V_{L_p} \leq V_{L_p}^{max}, p = 1, \ldots\ldots, NL \tag{48}$$

$$S_{l_q} \leq S_{l_q}^{max}, q = 1, \ldots\ldots, nl \tag{49}$$

FACTS devices bounds:

$$\tau_{\text{TCSCm}}^{min} \leq \tau_{TCSCm} \leq \tau_{\text{TCSCm}}^{max} \forall m \in N_{TCSC} \tag{50}$$

$$\phi_{\text{TCPSn}}^{min} \leq \tau_{TCPSn} \leq \tau_{\text{TCPSn}}^{max} \forall n \in N_{TCPS} \tag{51}$$

$$Q_{SVCj}^{min} \leq Q_{SVCj} \leq Q_{SVCj}^{max} \forall j \in N_{SVC} \tag{52}$$

The real power output limits of coal-based and wind units are shown in Equations (43) and (44), respectively. Then, Equations (45) and (46), which show the VAR power size of producing units, are used. The overall voltage regulator buses are shown in NG. PV bus voltage restrictions are shown in Equation (47), while PQ bus voltage restrictions are shown in Equation (48), where NL is the number of PQ buses. When NL is the total number of lines in a system, Equation (49) can be used to calculate line

loading limitations. Equations (50)–(52) show the limits of the TCSC, TCPS, and SVC devices, respectively.

4. Generalized Normal Distribution Optimization Algorithm

4.1. Inspiration

The normal distribution theory serves as the foundation for GNDO. The normal distribution, commonly referred to as the Gaussian distribution, is a crucial tool for describing natural phenomena. The following is a definition of a normal distribution. Assume that random variable x follows a probability distribution with location μ and scale δ parameters, and that its probability density function may be written as:

$$f(x) = \frac{1}{\sqrt{2\pi}\delta} exp\left(-\frac{(x-\mu)^2}{2\delta^2}\right) \tag{53}$$

Following that, x can be referred to as a normal random variable, and this distribution can be referred to as a normal distribution. Two variables, the location parameter and scale parameter, are part of a normal distribution, according to Equation (53). It is possible to describe the mean value and standard deviation of random variables using the location parameter and scale parameter, respectively. In general, population-based optimization approaches' search procedures consist of the three stages listed below. The scattered distribution contains all initialized people to start. Following that, everyone begins to move in the direction of the global optimal solution, and are guided by the designed exploration and exploitation tactics. The optimal answer is attained, and everyone congregates around it. Multiple normal distributions can adequately characterize this search process. To put it more precisely, individuals' positions can be thought of as random variables with a normal distribution. The ideal position and the mean position are farther apart in the initial stage. The positions of all people exhibit a significantly high standard deviation. The gap between the average and ideal positions gradually narrows in the second stage. With each individual's position, the standard variance decreases. The standard deviation of each individual's location can be as low as possible in the final stage, which also sees the shortest distance between the mean position and the ideal position.

4.2. Local Exploitation

The suggested GNDO framework is depicted in Figure 3. As can be seen, GNDO has a fairly straightforward structure, and its local exploitation and global exploration information exchange mechanisms are built specifically for GNDO. The generalized normal distribution model that has been constructed—which is based on the current mean position and the present optimal position—is the foundation for local exploitation. Three people that were chosen at random were tied to global exploration. The following provides a thorough overview of the two learning strategies. Local exploitation is the process of locating better solutions within a search space made up of everyone's present placements. A generalized normal distribution model for optimization can be constructed based on the correlation between the population's distribution of people and the normal distribution:

$$v_i^t = \mu_i + \delta_i \times \eta, i = 1, 2, 3, \ldots, N \tag{54}$$

where v_i^t is the trailing vector of the ith individual at time t, μ_i is the generalized mean position of the *i*th individual, δ_i is generalized standard variance, and η is the penalty factor. Moreover, μ_i, δ_i, and η can be defined as

$$\mu_i = \frac{1}{3}\left(x_i^t + x_{\text{Best}}^t + M\right) \tag{55}$$

$$\delta_i = \sqrt{\frac{1}{3}\left[\left(x_i^t - \mu\right)^2 + \left(x_{\text{Best}}^t - \mu\right)^2 + (M - \mu)^2\right]} \tag{56}$$

$$\eta = \begin{cases} \sqrt{-log(\lambda_1)} \times cos(2\pi\lambda_2), & \text{if } a <= b \\ \sqrt{-log(\lambda_1)} \times cos(2\pi\lambda_2 + \pi), & \text{otherwise} \end{cases} \tag{57}$$

where a, b, λ_1, and λ_2 are random numbers between 0 and 1, x_{Best}^t is the present fitness location, and M is the mean location of the present population. In addition, M can be calculated by:

$$M = \frac{\sum_{i=1}^{N} x_i^t}{N} \tag{58}$$

4.3. Global Exploration

A speech space is searched globally to identify promising regions. The worldwide exploration of GNDO is based on three individuals who were chosen at random, as shown in Figure 7.

$$v_i^t = x_i^t + \underbrace{\beta \times (|\lambda_3| \times v_1)}_{\text{Local information sharing}} + \underbrace{(1-\beta) \times (|\lambda_4| \times v_2)}_{\text{Global information sharing}} \tag{59}$$

where λ_3 and λ_4 are two random numbers subject to the standard normal distribution, β is called the adjust limit and is a random number between 0 and 1, and v_1 and v_2 are two trail vectors. Moreover, v_1 and v_2 can be calculated by:

$$v_1 = \begin{cases} x_i^t - x_{\text{p1}}^t, & \text{if } f(x_i^t) < f(x_{\text{p1}}^t) \\ x_{\text{p1}}^t - x_i^t, & \text{otherwise} \end{cases} \tag{60}$$

$$v_2 = \begin{cases} x_{\text{p2}}^t - x_{\text{p3}}^t, & \text{if } f(x_{\text{p2}}^t) < f(x_{\text{p3}}^t) \\ x_{\text{p3}}^t - x_{\text{p2}}^t, & \text{otherwise} \end{cases} \tag{61}$$

where p1, p2, and p3 are three random integers selected from 1 to N, which meets p1 $\neq$ p2 $\neq$ p3 $\neq$ i. In the context of Equations (60) and (61), the second term to the right of Equation (59) can be referred to as the local learning term, indicating that solution p1 shares information with solution *i*, and the third term to the right of Equation (59) can be referred to as the global information sharing term, indicating that the information is provided to the individual *i* by the individuals p2 and p3. To balance the two information-sharing options, *z* utilizes the adjusted parameter β. Furthermore, because λ_3 and λ_4 are random numbers with a typical normal distribution, the search space for the GNDO can be expanded when conducting a global search. The absolute symbol in Equation (59) is used to stay steady with the screening mechanism in Equations (60) and (61).
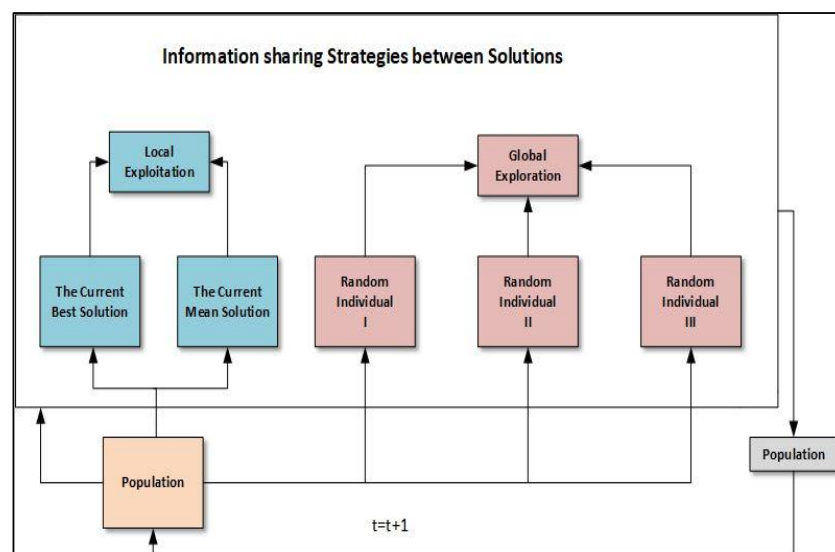
Figure 7. The framework of the proposed GNDO [25].

4.4. The Implementation of the Proposed Method for Optimization

This section presents the GNDO implementation. The defined local exploitation and global exploration tactics serve as the foundation for the proposed GNDO. The two tactics are equally important and equally likely to be chosen for the GNDO. Additionally, similar to other population-based optimization methods, GNDO initializes its population by;

$$x_{i,j}^t = l_j + \left(u_j - l_j\right) \times \lambda_5, i = 1, 2, 3, \ldots, N, j = 1, 2, 3, \ldots, D \tag{62}$$

where D is the total number of design variables, l_j is the jth design variable's lower boundary, u_j is its upper boundary, and λ_5 is a random number between 0 and 1. Note that neither a local exploitation approach nor a global exploration strategy will guarantee that the ith individual will find a better solution. A screening system is created to ensure that the population of the future generation receives the best solution, and it may be described as:

$$x_i^{t+1} = \begin{cases} v_i^t, & \text{if} f\left(v_i^t\right) < f\left(x_i^t\right) \\ x_i^t, & \text{otherwise} \end{cases} \tag{63}$$

Figure 8 provides the pseudocode of the GNDO.

```
START
INPUT: Define population size (N), limits on design variables (u, l), the current number of iteration t=0, and the
maximum number of iteration Tmax.
/* Initialization /*
Initialize the random generated population within its upper & lower bounds and evaluate it using Eq. (62).
find the fitness value of every individual and get the optimal solution xbest .
Modify the current iteration t by t=t+1;
/* Main Loop /*
while t ≤ Tmax do
  for i=1:N
          Generate the random number α between 0 and 1
    if α > 0.5 then
Local exploitation strategy*/
          select the current optimal solution xbest and calculate the mean position by M using Eq. (58)
          Compute the generalized mean position μ, Generalized standard deviation δ and penalty factor by
          Eq.(55), Eq. (56), and Eq. (57) respectively.
          Perform the local exploitation by Eq. (54) and Eq. (63) respectively.
          else
 Global exploration strategy*/
          Perform the global exploration strategy by Eq. (59), Eq. (60), Eq. (61) and Eq. (63) respectively.
          end if
      end for
      Update the current iteration t by t=t+1;
end while
OUTPUT: the optimal solution xbest.
```

Figure 8. The pseudocode of GNDO [25].

4.5. Basic Definitions of Multi-Objective Optimization

One optimization technique or tool that allows for more than one objective function to be used for any type of issue is multi-objective optimization. The following is a formulation of the fundamental elements of any multi-objective optimization:

$$
\left.
\begin{aligned}
\text{Minimize}: F\left(\vec{x}\right) &= \left[f_1\left(\vec{x}\right), f_2\left(\vec{x}\right), \ldots, f_o\left(\vec{x}\right)\right] \\
\text{Subjected to}: & \\
y_i\left(\vec{x}\right) &= 0, \quad i = 1, 2, \ldots, n \\
z_i\left(\vec{x}\right) &\geq 0, \quad i = 1, 2, \ldots, p \\
lb_i \leq x_i &\leq ub_i, \quad i = 1, 2, \ldots m
\end{aligned}
\right\}
\tag{64}
$$

where y_i signifies the ith equality constraint, z_i denotes the ith inequality constraint, n signifies the number of equality constraints, p denotes the number of inequality constraints, $\vec{x} = \left[\vec{x}_1, \vec{x}_2, \ldots, \vec{x}_j\right]^T$ denotes the decision/optimization variables, the minor and upper limits of the decision variables are represented by *lb* and *ub*, the number of decision variables is denoted by m, and the number of objective functions is denoted by o. In any multi-objective optimization problem, the relational operators are no longer valid to compare the search space solutions. The fundamental descriptions of multi-objective optimization problems are stated as follows, and a new operator known as Pareto optimality may be utilized to compare the solution.

Definition 1. *Pareto Optimality.*

The solution $\vec{x} \in X$ is called Pareto optimum if and only if:

$$
\nexists \, \vec{y} \in X \mid F\left(\vec{y}\right) \prec F\left(\vec{x}\right)
\tag{65}
$$

Definition 2. *Pareto Dominance.*

Let two different vectors be represented as $\vec{x} = (x_1, x_2, \ldots, x_j)$ and $\vec{y} = (y_1, y_2, \ldots, y_j)$. The vector $\vec{y}$ is said to dominate the vector $\vec{x}$ (symbolized as $\vec{y} \prec \vec{x}$), if and only if:

$$
\forall i \in \{1, 2, \ldots, j\}: f_i\left(\vec{y}\right) \leq f_i\left(\vec{x}\right) \wedge \exists i \in \{1, 2, \ldots, j\}: f_i\left(\vec{y}\right) < f_i\left(\vec{x}\right)
\tag{66}
$$

Definition 3. *Pareto Optimal Set.*

All Pareto optimal solution sets are called the Pareto set, and are expressed as follows:

$$
P_s = \left\{x, y \in X \mid \exists F\left(\vec{y}\right) \succ F\left(\vec{x}\right)\right\}
\tag{67}
$$

Definition 4. *Pareto Optimal Front.*

The Pareto optimal front is a collective of Pareto optimal solutions in the Pareto optimal set, as shown in (68):

$$
P_f = \left\{F\left(\vec{x}\right) \mid \vec{x} \in P_s\right\}
\tag{68}
$$

Any multi-objective optimization issue must be solved using the Pareto optimum set during the multi-objective optimization process. The search space (set of dominated solutions) and objective space (set of non-dominated solutions) are depicted in Figure 9. The Pareto optimum front describes the interaction between the objective space and search space.
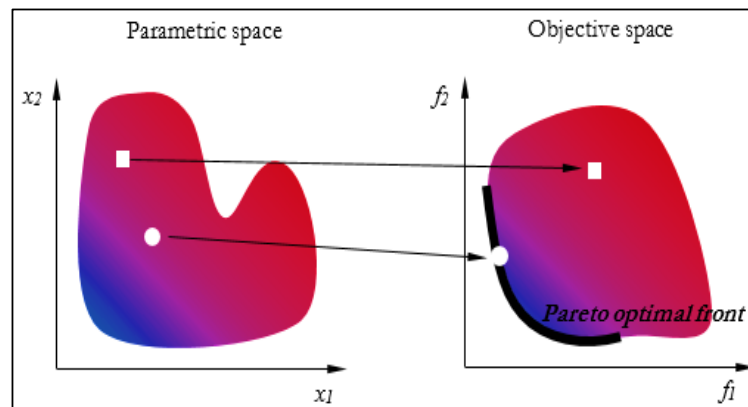
Figure 9. Objective space and search space in the multi-objective optimization problem.

4.6. Multi-Objective Generalized Normal Distribution Optimization (MOGNDO)

The proposed MOGNDO algorithm optimizer uses both the crowding distance (CD) mechanism and the elitist non-dominated sorting (NDS) method. The NDS consists of the following stages:

- Locating the non-dominated solution is the first step.
- The second step is the use of the NDS strategy.
- Performing non-dominated ranking (NDR) calculations on all non-dominated solutions.

Between two fronts, the NDR process takes place. The first front's solutions offer a "0" index because no solutions are dominated by them, but at least one solution from the first front dominates the second front's solutions. A solution's NDR is equal to the number of solutions that predominate it. The CD process is used to keep the created solutions diverse. The following is a definition of the CD mechanism:

$$CD_j^i = \frac{fobj_j^{i+1} - fobj_j^{i-1}}{fobj_j^{max} - fobj_j^{min}} \tag{69}$$

where $fobj_j^{max}$ and $fobj_j^{min}$ are the maximum and minimum values of jth objective function. The diagrammatic illustration of an NDS-based approach is illustrated in Figure 10.

The MOGNDO algorithm's pseudocode is displayed in Algorithm 1. The MOGNDO method begins by specifying the necessary inputs, such as population size (N_p), termination criteria, the maximum number of generations, and the maximum number of iterations (Maxit). Then, each objective function in the objective space vector F for P_o is evaluated using a randomly generated parent population P_o in the feasible search space region S. Thirdly, P_o is subjected to the elitist-based CD and NDS. Fourthly, P_o is merged with a fresh population of P_j to create a population, P_i. This P_i is sorted using the CD and NDR data, as well as elitist non-dominance. To establish a new parent population, the best N_p options are evaluated. The process is then repeated until the termination criteria are met. MOGNDO's flowchart is displayed in Figure 11.

Algorithm 1: Pseudocode of Multi-objective Generalized Normal Distribution Optimization (MOGNDO).

Step 1: Initially Generate population (P_o) randomly in solution space (S)
Step 2: Evaluate objective space (F) for the generated population (P_o)
Step 3: Sort the based on the elitist non-dominated sort method and find the non-dominated rank (NDR) and fronts
Step 4: Compute crowding distance (CD) for each front
Step 5: Update solutions (P_j)
Step 6: Merge P_o and P_j to create $P_i = P_o \cup P_j$
Step 7: For P_i perform **Step 2**
Step 8: Based on NDR and CD sort P_i
Step 9: Replace P_o with P_i for N_p first members of P_i

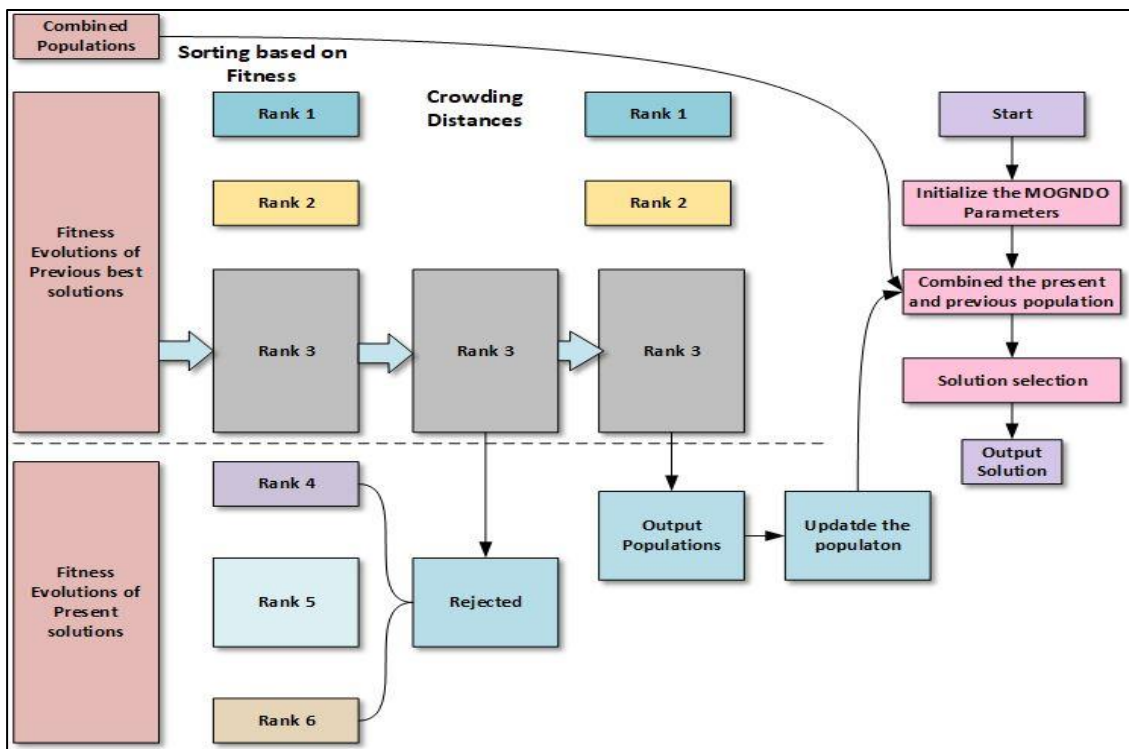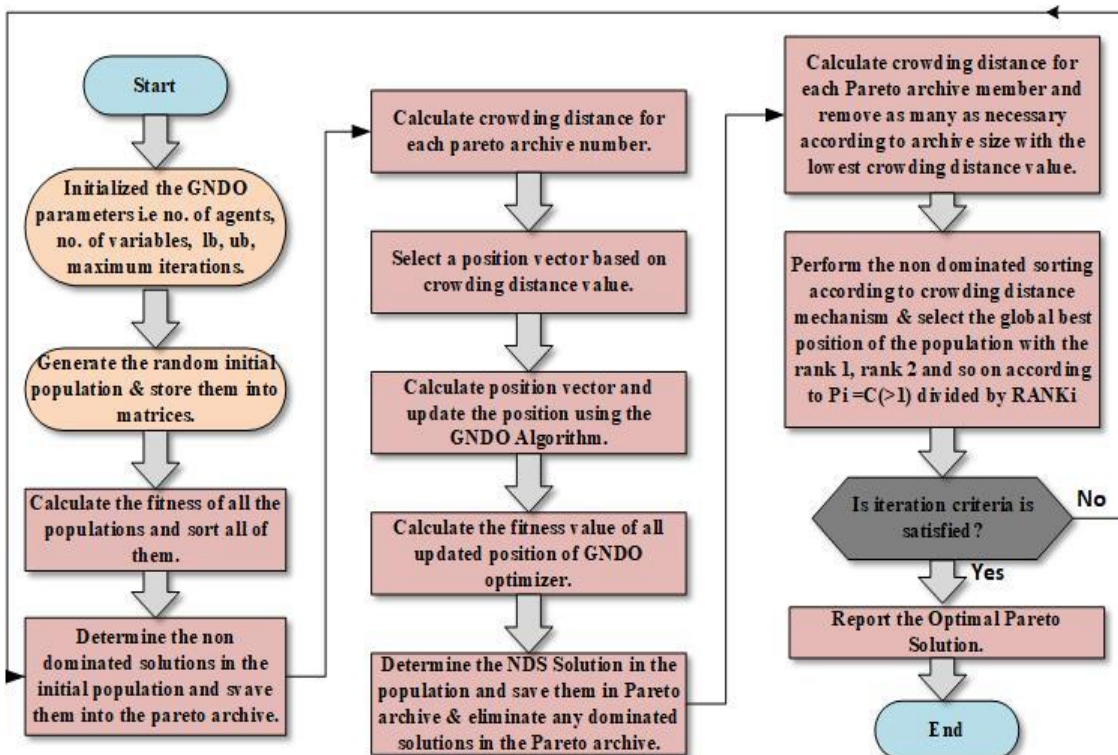**Figure 10.** The procedure of the non-dominated sorting approach.

Figure 11. Flowchart of MOGNDO algorithm.

4.7. Constraint Handling Approach

The majority of engineering design issues in the actual world are multi-objective and highly nonlinearly constrained. To solve constrained MOPs, managing all constraints within their bounds is crucial. A static penalty technique is used in the MOGNDO algorithm

because it transforms a constrained problem into an unconstrained problem, despite the literature survey giving various constrained handling approaches. This approach adds a significant penalty to the relevant goal function if a constraint is broken. The following is a presentation of the static penalty system:

$$f_j(X) = f_j(X) + \sum_{i=1}^{p} P_i \max\{g_i(X), 0\} + \sum_{i=p}^{NC} P_i \max\{|h_i(X)| - \delta, 0\} \tag{70}$$

where $f_j(X), j = 1, 2 \ldots n$ is the objective function to be optimized (here minimized), $X = \{x_1, x_2, \ldots x_m\}$ are design variables, $g_i(X) \leq 0, i = 1, 2 \ldots p$ are inequality constraints, $h_i(X) = 0, i = p + 1 \ldots NC$ are equality constraints, and δ is the tolerance in equality constraints.

4.8. Fuzzy Approach for the Multi-Objective Problem

The fuzzy membership approach can be used in multi-objective functions to identify the best compromising outcome out of all the non-inferior results. The fuzzy membership function μ_{f_i} uses a fuzzy membership function to keep track of the minimum f_i^{min} and maximum f_i^{max} values for each objective aim. Now, the membership function of the *i*th the objective is given as:

$$\mu_{f_i} = \begin{cases} 1 & f_i \leq f_i^{min} \\ \frac{f_i^{max} - f_i}{f_i^{max} - f_i^{min}} & f_i^{min} < f_i < f_i^{max} \\ 0 & f_i \geq f_i^{max} \end{cases} \tag{71}$$

The standards of membership functions lie on the measure of (0–1) and display in the way that satisfies the function f_i. Later, the decision-making function μ^k should be calculated as follows:

$$\mu^k = \frac{\sum_{i=1}^{N} \mu_{f_i}^k}{\sum_{k=1}^{M} \sum_{i=1}^{N} \mu_{f_i}^k} \tag{72}$$

For non-inferior findings, the decision-making function can also be thought of as the normalized membership function, which displays the ordering of the undominated results. The end outcome is regarded as the best attainable compromise among all PFs, with a maximum value of $maximum \left\{ \mu^k : k = 1, 2, 3 \ldots \ldots M \right\}$.

5. Simulation Results, Analysis, and Comparative Study

This section discusses the outcomes of the MOGNDO algorithm, which optimized the optimal power flow with non-conventional and FACTS device problems with control variables. The initialization of the algorithm's population size, archive size, the maximum number of iterations, and boundary condition for optimal power flow problems all came first. To identify the best optimal tradeoff points between multiple objective functions, the MOGNDO algorithm was then used to obtain the initial position and objective function values. Optimal power flow with non-conventional sources and FACTS devices were used to apply the MOGNDO algorithm's performance, which was initially verified on eight unconstrained multi-objective problems. On a computer with 4 GB of RAM and a 3.20 GHz clock speed, the simulation was run using the MATLAB program. The benchmark functions for each unconstrained test were solved using 10 separate runs. The population size was set to 30, the maximum number of iterations was set to 100, and the archive size was set to 30 when the control parameters for the proposed MOGWO algorithm were first set. The performance measures for the MOGNDO algorithm, including Generational Distance (GD), Inversion Generational Distance (IGD), Spacing Metrics (SP), Diversity Metrics (DM), and Spread Metrics (SD), are covered in this section.

5.1. MOGNDO Results for Test Benchmark Problems

Before tackling real-world issues, the MOGNDO was used to evaluate the performance of the benchmark unconstraint test function provided in [26]. Eight benchmark unconstrained test functions—ZDT1, ZDT2, ZDT3, ZDT4, ZDT6, KURSAVE, SCHAFFER-1, and SCHAFFER-2 (Figure 12) were taken into account, and a thorough simulation was performed using the MOGNDO technique. Any algorithm's control parameters are crucial to the resolution of the optimization problem. As a result, the number of populations was decided after conducting a comparative analysis that took into account various population sizes, while holding all other variables constant. Following careful consideration, the population size, maximum iterations, and archive size were chosen as 30, 100, and 30, respectively, for the unconstrained test benchmark functions. The MOGNDO algorithm's performance was evaluated using performance metrics, such as Generational Distance (GD), Inversion Generational Distance (IGD), Spacing Metrics (SP), Diversity Metrics (DM), and Spread Metrics (SD), for convergence measurement. Tables 3–7 demonstrate that MOGNDO could achieve the best outcomes for all performance metrics, including Generational Distance (GD), Inversion Generational Distance (IGD), Spacing Metrics (SP), Diversity Metrics (DM), and Spread Metrics (SD), which cover convergence and solution accuracy. It follows that the suggested MOGNDO can provide the best convergence on all benchmark functions. The outcomes (archive solutions) of all eight test benchmark issues are displayed in Figures 1–5. As can be shown, the MOGNDO method was capable of approximating the PF. By comparing the PF estimations, it can also be seen that the suggested MOGNDO could provide acceptable performance. Thus, it was determined that the MOGNDO algorithm is more suitable for the stochastic OPF problem with three FACTS devices and wind power plants.

Table 3. Results of $GDMETRICS$ on test functions.

TEST FUNCTIONS	Minimum	Average	Median	Maximum	Std Dev
ZDT-1	0.00014795	0.00025051	0.00025043	0.00033133	6.658×10^{-5}
ZDT-2	0.00015293	0.00016665	0.00016915	0.00018271	8.9928×10^{-6}
ZDT-3	0.00048314	0.00059601	0.00057943	0.00077354	9.9396×10^{-5}
ZDT-4	0.00012104	0.00022808	0.00020834	0.0004758	9.4401×10^{-5}
ZDT-6	9.084×10^{-5}	0.046963	0.00011316	0.22777	0.084189
KURSAVE	0.00079741	0.0014452	0.0012905	0.0025211	0.00051722
SCHAFFER-1	0.00033607	0.00040992	0.00042203	0.00047897	4.714×10^{-5}
SCHAFFER-2	4.3236×10^{-5}	7.2824×10^{-5}	5.2463×10^{-5}	0.00016939	4.0743×10^{-5}

Table 4. Results of $IGD\ METRICS$ on test functions.

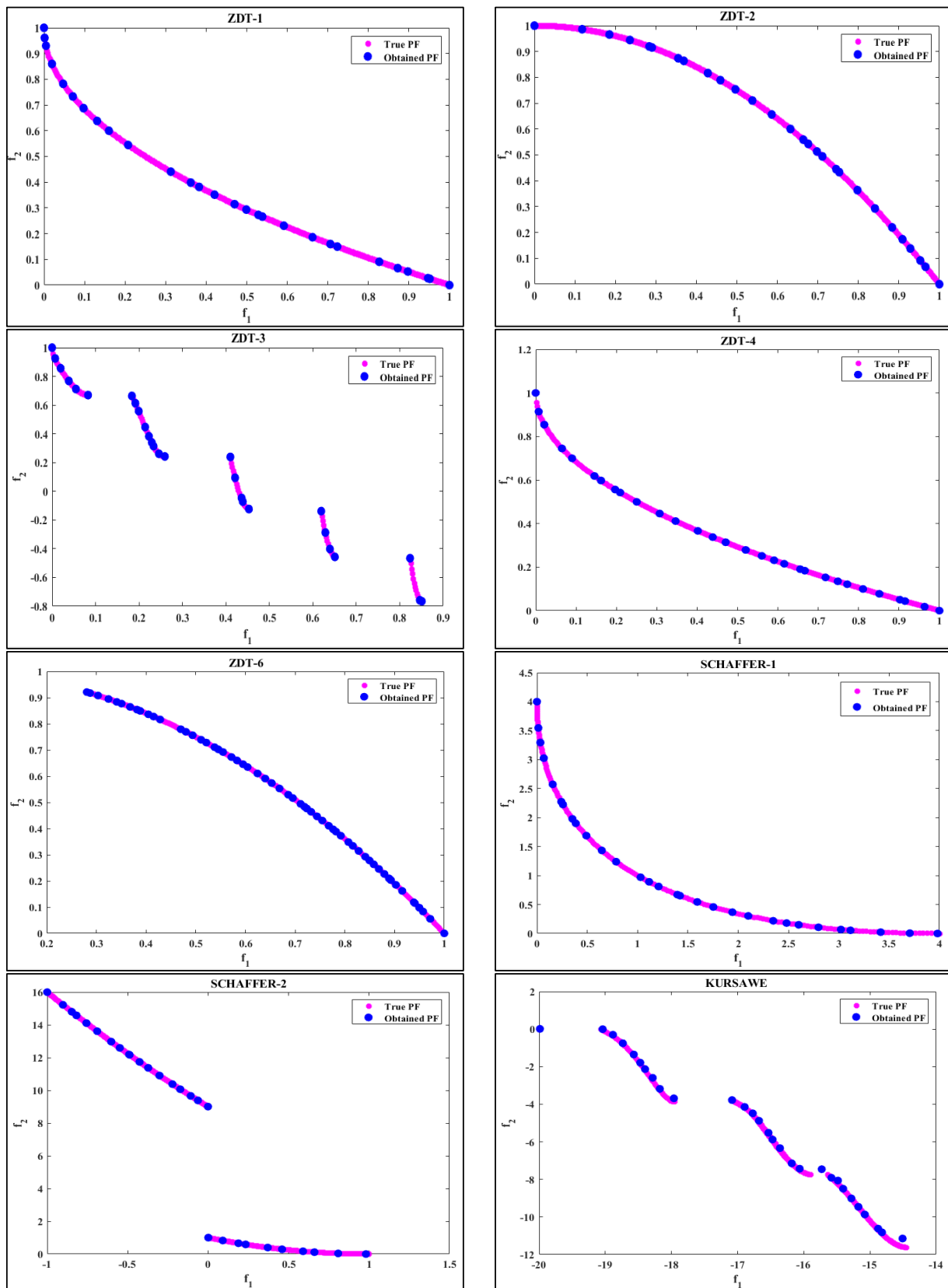| TEST FUNCTIONS	Minimum	Average	Median	Maximum	Std Dev
ZDT-1	0.00086623	0.00098862	0.0010348	0.0010718	8.6005×10^{-5}
ZDT-2	0.00086578	0.00098848	0.00094837	0.0012358	0.00012678
ZDT-3	0.001211	0.0020746	0.0013386	0.0077205	0.0020015
ZDT-4	0.00078066	0.00089518	0.00087008	0.0012276	0.00012621
ZDT-6	0.0004207	0.00045525	0.00044688	0.00049748	2.8268×10^{-5}
KURSAVE	0.00054436	0.00062399	0.00057845	0.00085408	9.8135×10^{-5}
SCHAFFER-1	0.0013154	0.0015246	0.0015027	0.0017064	0.0001302
SCHAFFER-2	0.00038808	0.00042594	0.00042586	0.00044933	1.8173×10^{-5}

Figure 12. Best Pareto optimal front obtained of unconstrained test functions by MOGNDO algorithm.

Table 5. Results of *SPACINGMETRICS* on test functions.

TEST FUNCTIONS	Minimum	Average	Median	Maximum	Std Dev
ZDT-1	0.055513	0.068922	0.068773	0.078086	0.0087192
ZDT-2	0.055269	0.066982	0.06225	0.082706	0.010406
ZDT-3	0.23708	0.30199	0.30489	0.37195	0.038816
ZDT-4	0.055461	0.079673	0.082798	0.0984	0.012829
ZDT-6	0.060275	0.36467	0.082672	1.2984	0.50689
KURSAVE	1.7123	2.0817	2.0541	2.3807	0.20644
SCHAFFER-1	0.47734	0.6444	0.65722	0.78476	0.086121
SCHAFFER-2	4.3184	6.228	6.1458	8.1797	0.99173

Table 6. Results of *DIVERSITYMETRICS* on test functions.

TEST FUNCTIONS	Minimum	Average	Median	Maximum	Std Dev
ZDT-1	0.39774	0.4726	0.46959	0.53772	0.060856
ZDT-2	0.34666	0.4369	0.44215	0.57139	0.069382
ZDT-3	0.42402	0.52122	0.50625	0.64813	0.07401
ZDT-4	0.3035	0.37573	0.36822	0.43095	0.043003
ZDT-6	0.36148	0.6907	0.45236	1.3455	0.42847
KURSAVE	0.28774	0.3839	0.39009	0.45763	0.050257
SCHAFFER-1	0.28774	0.3839	0.39009	0.45763	0.050257
SCHAFFER-2	0.9161	0.95607	0.95992	1.0033	0.030768

Table 7. Results of *SPREAD METRICS* on test functions.

TEST FUNCTIONS	Minimum	Average	Median	Maximum	Std Dev
ZDT-1	0.38649	0.45794	0.45049	0.5251	0.059019
ZDT-2	0.33511	0.42459	0.42842	0.56709	0.070091
ZDT-3	0.5604	0.64503	0.64749	0.73814	0.066426
ZDT-4	0.30364	0.36741	0.36204	0.4213	0.040601
ZDT-6	0.35291	0.67963	0.4479	1.3293	0.42341
KURSAVE	0.37729	0.43491	0.43448	0.4872	0.030263
SCHAFFER-1	0.27113	0.37375	0.37832	0.44441	0.051198
SCHAFFER-2	0.56431	0.61293	0.61561	0.65022	0.02504

5.2. Multi-Objectives OPF Problem with Wind Power Plants and Three FACTS Devices

The GNDO algorithm was used to address the stochastic OPF problem with wind power plants and three FACTS devices in this study. The solution to the optimum power flow problem was evaluated in parallel using newly created algorithms, such as the Multi-Verse Optimization (MVO), the Sine-Cosine Algorithm (SCA) [27], the Grey Wolf Optimization (GWO), the Moth Fame Optimization (MFO), the Ant Lion Optimization (ALO) [28], and Ion Motion Algorithms (IMA) [29]. The proposed approach was demonstrated using a modified IEEE-30 bus infrastructure with wind power plants and FACTS devices. Table 1 lists the major characteristics of the customized IEEE-30 bus framework. The following are two scenarios:

- Scenario-1 (Solo objective OPF with wind power plants and FACTS devices)
- Scenario-2 (Multi-objective OPF with wind power plants and FACTS devices)

As shown in Table 8, there were a total of thirteen different test scenarios to evaluate. In this section, the results of case studies using various metaheuristics methodologies are tabulated and presented. The first six case studies are for single-objective optimization, while the latter seven are multi-objective optimization problems that include non-conventional sources of energy resources, as well as optimal FACTS device sizes and locations. The search agent value was set to 40, and each algorithm underwent 500 iterations of analysis. Please refer to the original research for a detailed discussion of those procedures. Table 4 shows the parameter settings for these methods.

Table 8. Summary of case studies for adapted IEEE-30 bus test system.

Test System	Case #	Single and Multi-Objectives Functions
	Case # 1	TFC includes FACTS devices, wind farms, and coal-based plants
	Case # 2	Reduction of total toxic gas emanations with the use of coal-based, wind, and FACTS technologies.
	Case # 3	Minimization of APL in FACTS devices, wind farms, and coal-based plants.
	Case # 4	Minimization of the total voltage variation using coal-based, wind, and FACTS devices.
	Case # 5	Voltage stability improvement in coal-based, wind, and FACTS equipment.
	Case # 6	Total Gross Generation Cost, includes FACTS devices, wind farms, and coal-based plants.
Adapted IEEE 30-bus test system	Case # 7	Minimizing TFCs and toxic gas emanations while using non-conventional sources of energy and FACTS devices
	Case # 8	TFC and APL Minimization Including non-conventional sources and FACTS Devices
	Case # 9	TFC and VSI minimization including non-conventional sources and FACTS devices
	Case # 10	Total Gross Generation Cost and voltage deviation minimization with non-conventional sources and FACTS devices
	Case # 11	TFC, Toxic gas emanation, and APL minimization together with non-conventional sources and FACTS devices
	Case # 12	TFC, APL, and VSI minimization including non-conventional sources and FACTS devices
	Case # 13	TFC, Toxic gas emanation, APL, and voltage deviation minimization including non-conventional sources and FACTS devices

5.3. Scenario-1 (Single Objective OPF with Wind Power Plants and FACTS Devices)

With the use of GNDO, MVO, ALO, SCA, and IMO methods, all of the objective goals indicated in the mathematical formulation were simultaneously handled as solo objective optimization issues. The limitations of all control variables, as well as proper FACTS device locations and sizing, are listed below. From case 1 to case 6, the outcomes of objective functions are tabulated in Tables 9–11, with the best minimum values containing five different recent techniques.

Table 9. Single objectives simulation results for case 1 and case 2.

Control & State Variables	Min	Max	Case-1					Case-2				
			GNDO	MVO	ALO	SCA	IMO	GNDO	MVO	ALO	SCA	IMO
PTG2	20	80	41.427	40.311	40.960	35.458	30.881	46.634	46.639	46.634	48.357	46.726
PWG5	0	75	49.815	49.459	49.077	41.719	54.226	74.818	74.934	71.362	75.000	74.507
PTG8	10	35	10.000	10.352	13.038	15.172	14.361	35.000	35.000	35.000	35.000	35.000
PWG11	0	60	40.799	42.135	39.362	47.561	36.329	52.365	51.215	54.905	60.000	48.761
PTG13	12	40	12.002	12.000	12.000	14.321	16.648	40.000	40.000	40.000	40.000	40.000
V1	0.95	1.1	1.091	1.100	1.100	1.019	1.100	1.090	0.997	1.100	0.997	1.100
V2	0.95	1.1	1.075	1.090	1.091	0.992	1.100	1.080	1.013	1.078	0.950	1.100
V5	0.95	1.1	1.049	1.071	1.072	0.978	1.100	1.067	1.037	0.975	1.100	1.100
V8	0.95	1.1	1.046	1.076	1.079	0.950	1.100	0.962	1.100	1.100	1.100	1.100
V11	0.95	1.1	1.100	1.100	1.071	1.047	1.100	1.073	1.082	1.100	0.950	1.100
V13	0.95	1.1	1.069	1.062	1.038	0.950	1.100	1.087	0.970	1.047	1.100	1.100
T11	0.9	1.1	1.037	1.007	1.059	0.959	1.090	0.977	0.938	1.020	1.100	1.100
T12	0.9	1.1	0.997	1.087	1.084	0.900	1.090	0.943	1.055	1.073	0.965	1.100
T15	0.9	1.1	1.027	1.099	1.095	0.938	1.090	1.023	1.063	1.080	0.900	1.100
T36	0.9	1.1	0.957	1.024	1.087	0.900	1.090	1.017	1.024	1.054	0.900	1.100
SVC1 Location	-	-	24	27	6	19	22	27	11	21	25	29
SVC2 Location	-	-	7	27	10	9	15	6	20	30	25	30
SVC1 Rating	−10	10	10.000	9.893	−6.541	3.882	1.740	−3.380	9.274	8.786	10.000	10.000
SVC2 Rating	−10	10	5.764	−6.277	1.209	5.482	−3.094	−9.559	0.639	8.550	−10.000	4.480
TCSC1 Location	-	-	15	39	10	3	14	37	38	32	34	33
TCSC2 Location	-	-	12	29	20	4	32	36	24	37	41	39
TCSC1 Rating	0	0.5	0.491	0.219	0.218	0.000	0.452	0.110	0.196	0.497	0.000	0.500
TCSC2 Rating	0	0.5	0.496	0.239	0.440	0.000	0.492	0.454	0.060	0.485	0.193	0.500
TCPS1 Location	-	-	14	16	34	15	14	38	14	26	40	40
TCPS2 Location	-	-	16	22	19	1	30	35	5	32	1	41
TCPS1 Rating	−5	5	2.714	4.503	−3.990	3.917	1.235	4.787	−0.175	0.926	5.000	5.000
TCPS2 Rating	−5	5	1.705	3.761	−4.281	1.150	0.113	4.095	1.148	4.860	−3.963	4.566
TFC ($/h)			806.999	808.030	809.449	818.654	814.865	-	-	-	-	-
Emission (Ton/h)			-	-	-	-	-	0.138	0.138	0.138	0.138	0.138

Table 10. Single objectives simulation results for case 3 and case 4.

Control & State Variables	Min	Max	Case-3					Case-4				
			GNDO	MVO	ALO	SCA	IMO	GNDO	MVO	ALO	SCA	IMO
PTG2	20	80	69.005	75.900	79.745	80.000	79.644	79.721	78.271	28.577	49.606	34.817
PWG5	0	75	75.000	74.966	75.000	73.825	74.667	47.504	11.236	13.419	0.000	47.506
PTG8	10	35	34.999	34.656	35.000	30.726	34.844	25.357	32.736	16.328	35.000	34.441
PWG11	0	60	59.999	58.422	60.000	50.635	59.748	26.234	20.292	4.602	0.000	55.391
PTG13	12	40	39.976	31.239	39.823	31.706	39.832	26.916	32.996	24.669	24.060	39.576
V1	0.95	1.1	1.036	1.100	1.098	1.098	1.089	1.008	0.958	0.967	0.950	0.955
V2	0.95	1.1	1.037	1.100	1.100	1.091	1.089	1.032	1.054	1.051	1.072	1.052
V5	0.95	1.1	1.027	1.090	1.091	1.100	1.089	1.010	1.016	1.017	0.960	0.955
V8	0.95	1.1	1.030	1.092	1.096	1.100	1.090	1.025	0.992	1.013	1.024	1.015
V11	0.95	1.1	1.100	1.099	1.100	1.100	1.089	0.950	1.069	1.009	1.100	1.004
V13	0.95	1.1	1.100	1.100	1.077	0.990	1.089	1.004	1.067	1.084	1.043	1.038
T11	0.9	1.1	1.012	1.047	1.046	1.030	1.090	0.938	1.063	0.949	1.017	0.905
T12	0.9	1.1	0.903	0.903	1.045	1.100	1.090	0.907	0.903	0.904	0.912	0.986
T15	0.9	1.1	0.998	1.042	1.100	1.018	1.090	0.945	1.048	1.065	1.044	1.069
T36	0.9	1.1	0.935	0.983	1.068	1.100	1.090	0.934	0.930	0.936	0.957	0.936
SVC1 Location	-	-	18	12	27	11	27	19	24	28	19	19
SVC2 Location	-	-	24	15	30	16	30	10	14	16	21	23
SVC1 Rating	−10	10	4.901	6.871	3.951	6.535	9.956	8.082	8.769	−1.898	4.969	9.593
SVC2 Rating	−10	10	10.000	5.448	5.238	−0.936	4.219	5.421	−2.342	−5.291	−1.465	9.547
TCSC1 Location	-	-	34	5	40	3	40	14	13	2	2	40
TCSC2 Location	-	-	11	40	41	2	41	18	25	9	5	29
TCSC1 Rating	0	0.5	0.494	0.107	0.500	0.000	0.471	0.353	0.300	0.075	0.027	0.500
TCSC2 Rating	0	0.5	0.500	0.198	0.497	0.000	0.498	0.499	0.391	0.087	0.000	0.486
TCPS1 Location	-	-	16	12	40	4	33	19	38	3	1	37
TCPS2 Location	-	-	19	15	41	1	34	15	41	5	5	36
TCPS1 Rating	−5	5	1.744	−0.898	−3.378	0.433	4.979	−4.997	3.754	−1.638	5.000	2.660
TCPS2 Rating	−5	5	0.257	4.748	−3.441	1.249	0.946	0.767	0.550	−3.874	0.128	−1.703
APL (MW)			1.647	1.735	1.686	2.482	1.880	-	-	-	-	-
Voltage Deviation (p.u)			-	-	-	-	-	0.124	0.150	0.177	0.227	0.165

Table 11. Single objectives simulation results for case 5 and case 6.

Control & State Variables	Min	Max	Case-5					Case-6				
			GNDO	MVO	ALO	SCA	IMO	GNDO	MVO	ALO	SCA	IMO
PTG2	20	80	78.161	28.765	76.487	20.000	74.363	44.894	47.802	55.203	20.000	56.164
PWG5	0	75	75.000	16.020	74.240	0.000	67.677	74.998	74.564	71.256	75.000	68.555
PTG8	10	35	35.000	34.855	34.405	10.000	32.815	35.000	32.893	33.271	35.000	30.826
PWG11	0	60	54.355	0.000	55.983	49.379	14.173	59.006	58.030	50.102	60.000	58.732
PTG13	12	40	12.001	28.840	38.080	16.659	35.961	21.583	22.222	32.274	19.540	23.229
V1	0.95	1.1	1.100	1.100	1.100	1.100	1.097	1.046	1.100	1.100	1.100	1.100
V2	0.95	1.1	1.100	1.100	1.100	1.100	1.097	1.042	1.097	1.098	1.100	1.100
V5	0.95	1.1	1.100	1.100	1.100	1.100	1.097	1.032	1.087	1.087	1.100	1.100
V8	0.95	1.1	1.100	1.100	1.100	1.100	1.097	1.035	1.092	1.091	1.100	1.098
V11	0.95	1.1	1.100	1.100	1.100	1.100	1.097	1.098	1.100	1.100	1.100	1.100
V13	0.95	1.1	1.100	1.100	1.100	1.100	1.097	1.035	1.100	1.083	1.100	1.098
T11	0.9	1.1	0.905	0.910	0.990	1.100	1.089	1.077	1.054	1.007	1.100	1.084
T12	0.9	1.1	0.904	0.909	0.990	0.900	1.089	0.901	0.903	1.089	1.100	1.084
T15	0.9	1.1	0.901	0.900	0.930	0.900	1.089	1.065	1.053	1.081	1.100	1.100
T36	0.9	1.1	0.901	0.909	0.910	0.900	0.910	0.985	1.001	1.033	1.100	1.087
SVC1 Location	-	-	10	29	29	29	26	24	28	26	15	24
SVC2 Location	-	-	29	30	30	30	26	13	14	26	3	10
SVC1 Rating	−10	10	9.999	4.260	7.322	10.000	9.312	9.999	−3.639	3.886	10.000	8.490
SVC2 Rating	−10	10	9.999	2.982	9.608	9.747	9.622	3.844	−1.487	3.411	−0.065	7.591
TCSC1 Location	-	-	38	38	38	24	36	16	7	39	1	18
TCSC2 Location	-	-	15	36	40	1	38	19	29	34	3	31
TCSC1 Rating	0	0.5	0.500	0.490	0.500	0.002	0.499	0.500	0.468	0.470	0.002	0.500
TCSC2 Rating	0	0.5	0.500	0.325	0.475	0.013	0.499	0.013	0.490	0.355	0.000	0.147
TCPS1 Location	-	-	36	4	33	3	38	14	4	35	31	30
TCPS2 Location	-	-	41	17	38	1	39	4	2	25	11	33
TCPS1 Rating	−5	5	−4.999	3.788	4.884	−5.000	4.540	3.173	0.486	4.591	2.761	1.494
TCPS2 Rating	−5	5	−4.998	1.993	4.772	−1.126	4.697	−0.508	−1.527	−0.901	5.000	2.191
VSI			0.096	0.100	0.096	0.108	0.102	-	-	-	-	-
Total Gross Fuel Cost ($/h)			-	-	-	-	-	1120.996	1125.970	1138.357	1187.287	1148.359

The overall fuel cost with GNDO, which included the two non-conventional sources of power plants and optimal placement of FACTS devices, was 806.999 $/h, which was the best in comparison with the other cited algorithm shown in Table 9. The reductions in TFC in comparison with MVO, ALO, SCA, IMO, SHADE-SF, DE-SF, ABC-SF, PSO-SF, FPA-SF, and MSA-SF were 1.031 $/h, 1.031 $/h, 2.45 $/h, 11.655 $/h 7.866 $/h, 0.0176 $/h, 0.4917 $/h, 0.4 $/h, 1.2553 $/h, 3.398 $/h, and 1.0403 $/h, respectively. This demonstrated the GNDO algorithm's superiority over other cited metaheuristics algorithms.

Figure 13 illustrates the convergence traits of the TFC minimization. Similar convergence traits for APL, voltage deviations, and VSI are depicted in Figures 14–16. Figure 17 also displays a comparison of the fuel cost decrease with various algorithms. In example 2, the GNDO method resulted in a pollutant gas emission of 0.138 tons per hour. In instance 3, the APL of the various transmission lines using the GNDO approach was 1.647 MW. The APL was 0.088 MW, 0.039 MW, 0.835 MW, 0.233 MW, 0.0997 MW, 0.0997 MW, 0.2598 MW, 0.2494 MW, 0.6127 MW, and 0.4972 MW less compared to MVO, ALO, SCA, IMO, SHADE-SF, DE-SF, ABC-SF, PSO-SF, and MSA-SF, respectively. A crucial factor for the grid's ability to operate reliably was the voltage divergence of each bus from 1.0 per unit. Therefore, in scenario 4, the moth flame algorithm produced the lowest voltage variation (0.124 p.u), making it the best of the five optimization methods. The VSI, sometimes referred to as the L max index, varied between zero (no load) and one (voltage collapse). Therefore, in case 5, 0.096 was the lowest value for the L max index. In scenario 6, the overall gross fuel cost using the GNDO method was 1120.996 dollars per hour. It is interesting to note here that in Table 12, the total gross fuel cost of the proposed GNDO was more than the SHADE-SF, which further enforces the narrative of the "No free lunch theorem," which states that no algorithm gives the best result in every problem.
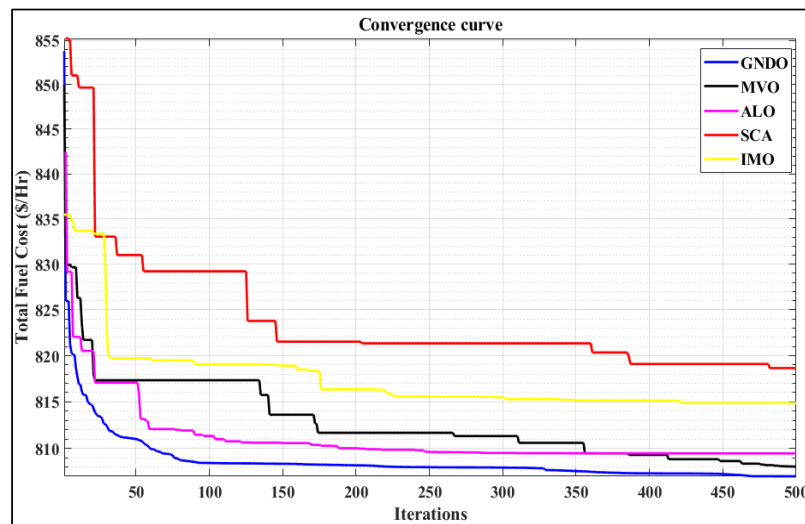

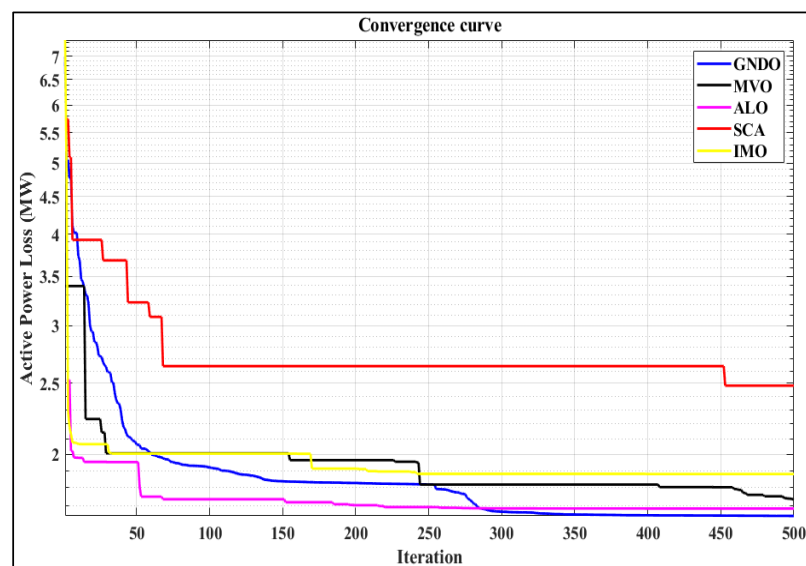**Figure 13.** Convergence characteristics of TFC minimization.

Figure 14. Convergence characteristics of APL minimization.
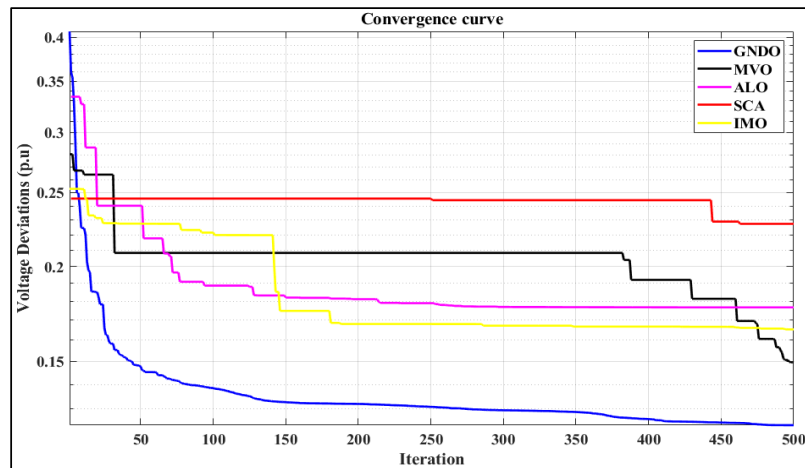
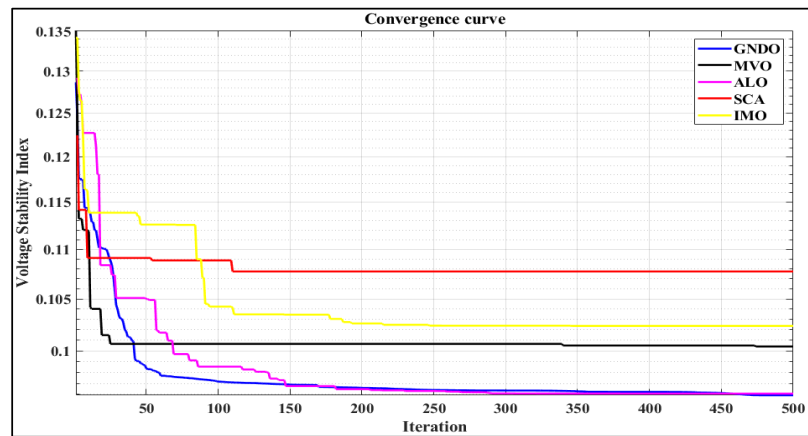**Figure 15.** Convergence characteristics of voltage deviation minimization.

Figure 16. Convergence characteristics of VSI minimization.
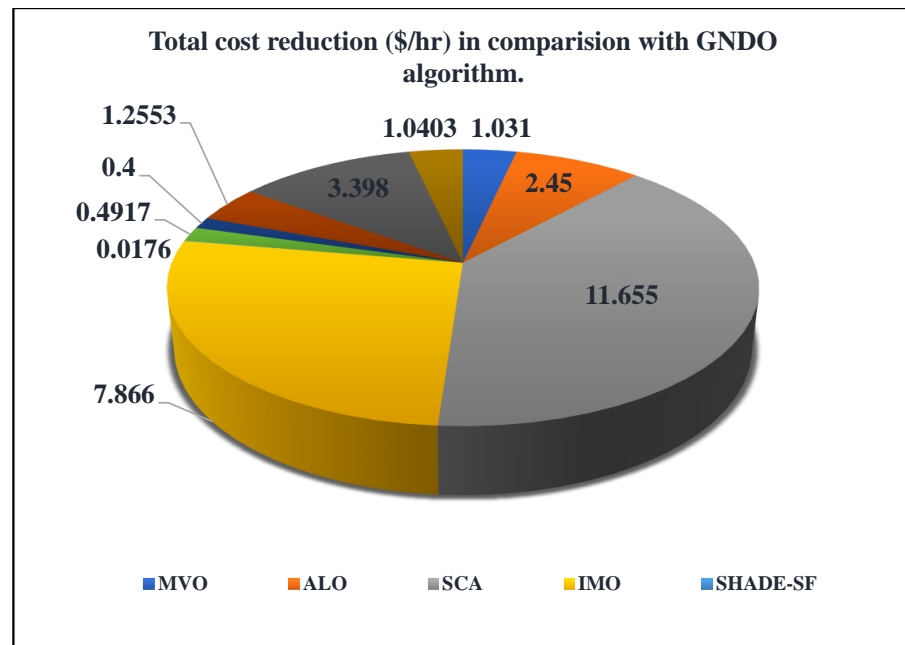
Figure 17. Comparison of the TFC reduction ($/h) with other algorithms.

Table 12. Comparison of the simulation results for single objectives.

Objectives Functions	GNDO	MVO	ALO	SCA	IMO	SHADE-SF	DE-SF	ABC-SF	PSO-SF	FPA-SF	MSA-SF
Total F.C ($/h)	806.999	808.030	809.449	818.654	814.865	807.0166	807.4907	807.399	808.2543	810.397	808.0393
Emission (T/h)	0.138	0.138	0.138	0.138	0.138	-	-	-	-	-	-
Ploss (MW)	1.647	1.735	1.686	2.482	1.880	1.7467	1.7467	1.9068	1.8964	2.2597	2.1442
V.D (p.u)	0.124	0.150	0.177	0.227	0.165	-	-	-	-	-	-
Lmax	0.096	0.100	0.096	0.108	0.102	-	-	-	-	-	-
Total Gross F.C ($/h)	1120.996	1125.970	1138.357	1187.287	1148.359	1104.077	1113.676	1116.365	1118.601	1164.719	1122.331

Figures 18 and 19 provide comparison charts with the minimizing of APL and overall fuel cost. The results of the simulations were compared to those of the most recent algorithms, including MVO, ALO, SCA, IMO, and other mentioned optimization approaches. It was found that the proposed method of Generalized Normal Distribution Optimization methodology produced superior results.

Figure 18. Comparison chart for TFC minimization with different algorithms.

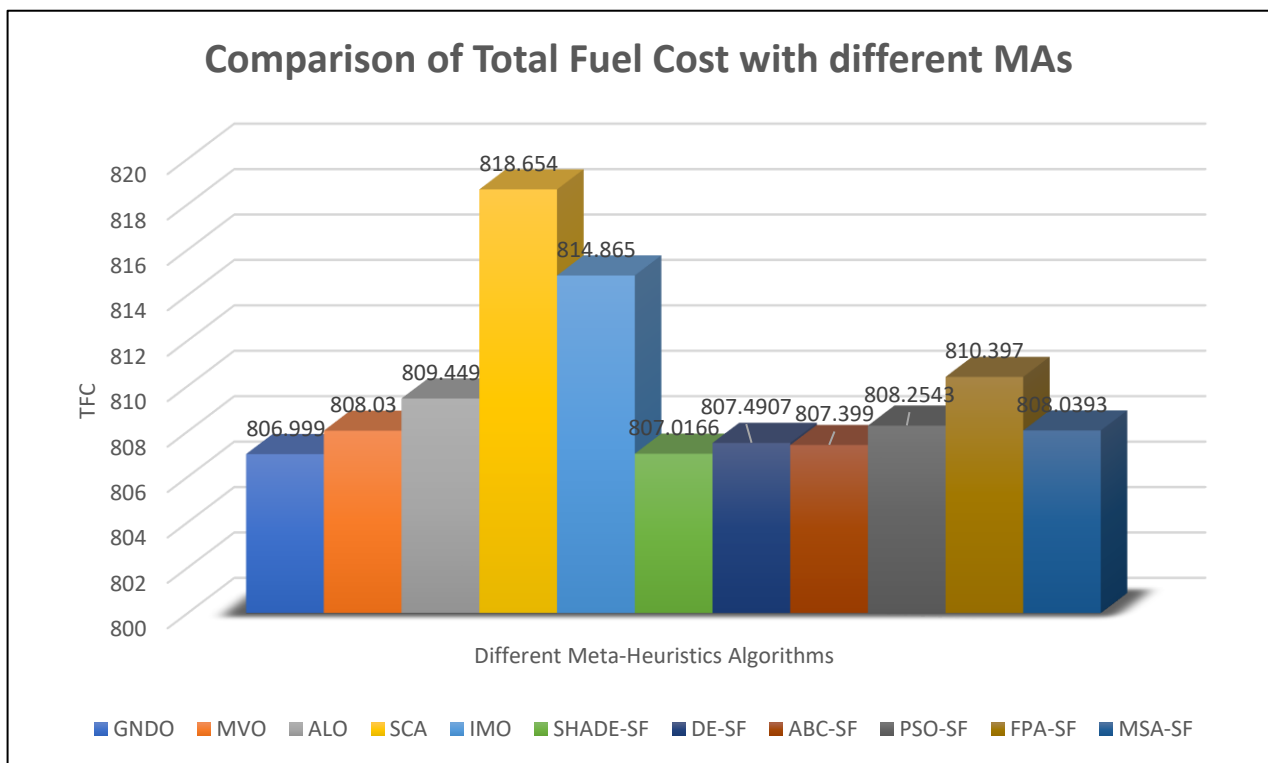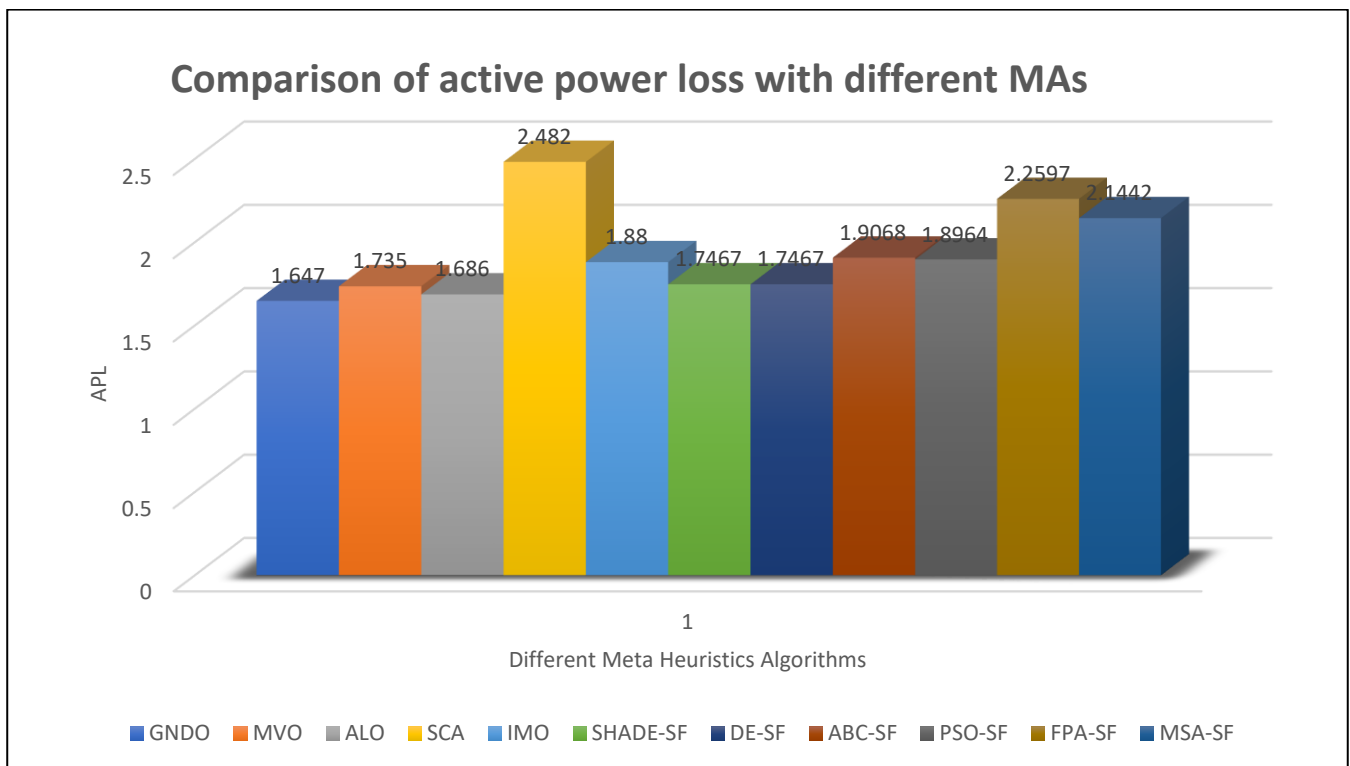**Figure 19.** Comparison chart for APL minimization with different algorithms.

5.4. Scenario-2 (Multi-Objective OPF with Non-Conventional Sources Energy Resources)

In this case, two, three, and four objectives were simultaneously optimized using the Multi-Objective Generalized Normal Distribution Optimization (MOGNDO) algorithm technique. In multi-objective optimization, the non-dominated sorting optimization technique is used to simultaneously find solutions for numerous objectives. To find the PF for the modified IEEE 30-bus architecture, 30 non-dominate solutions are retained. The scenarios in cases 7 through 10 are thought of as two-objective optimization cases. Three-objective optimization problems are what are known as cases 11 and 12. Contrarily, case 13 is referred to as a set of four problems involving objective optimization. Among all the Pareto archives, the best compromising solution was found using the fuzzy decision-making method. For cases 7 through 13, the most optimal compromise solutions using the proposed MOGNDO algorithm and other cited metaheuristics techniques are shown in boldface and stated in Tables 13–16. The best PFs of TFC and pollution minimization for case 7 are shown in Figure 20, utilizing various metaheuristics techniques. Likewise with case 7, case 8's PF with two goal optimizations resulted in APL and TFC, which are depicted in Figure 21. Figure 22 shows the PF of the TFC with the carbon tax and voltage deviation minimization. In scenario 11, Figure 23 shows the three objectives PFs for minimizing APL, TFC, and toxic gas emanations. Figure 24 depicts the PF for the minimization of voltage variation, APL, and TFC, using various algorithms.

Table 13. Multi-objective simulation results for case 7 and case 8.

Control & State Variables	Min	Max	Case-7				Case-8			
			GNDO	**GWO**	**MFO**	**MVO**	**GNDO**	**GWO**	**MFO**	**MVO**
PTG2	**20**	**80**	45.896	54.592	47.915	47.568	31.212	44.406	40.200	37.027
PWG5	**0**	**75**	54.828	58.922	53.220	52.055	64.776	65.069	60.990	63.027
PTG8	**10**	**35**	23.322	20.821	25.403	24.401	17.913	23.015	25.019	24.049
PWG11	**0**	**60**	46.878	42.848	41.484	46.116	48.381	51.171	51.429	43.893
PTG13	**12**	**40**	19.171	17.914	22.285	22.094	14.453	23.604	19.015	14.758
V1	**0.95**	**1.1**	1.031	1.043	1.067	1.036	1.085	1.099	1.087	1.065
V2	**0.95**	**1.1**	1.027	1.019	1.055	1.025	1.075	1.090	1.082	1.049
V5	**0.95**	**1.1**	1.022	1.000	1.029	1.010	1.057	1.077	1.069	1.027
V8	**0.95**	**1.1**	1.023	1.001	1.032	1.020	1.054	1.071	1.074	1.041
V11	**0.95**	**1.1**	1.031	1.035	1.039	1.022	1.087	1.077	1.073	1.069
V13	**0.95**	**1.1**	1.026	1.020	1.045	1.029	1.075	1.079	1.052	1.037
T11	**0.9**	**1.1**	0.986	0.956	1.007	0.987	0.972	1.003	1.034	1.016
T12	**0.9**	**1.1**	1.006	0.966	1.002	1.001	1.020	1.037	1.045	0.966
T15	**0.9**	**1.1**	1.041	0.953	1.051	1.038	1.049	1.071	1.057	1.017
T36	**0.9**	**1.1**	1.003	0.956	1.012	0.981	0.990	0.996	1.033	1.004
SVC1 Location	–	–	15	11	15	14	12	22	16	19
SVC2 Location	–	–	22	25	19	10	17	12	23	13
SVC1 Rating	−**10**	**10**	0.696	0.846	−1.633	2.629	−0.018	8.596	−3.998	6.891
SVC2 Rating	−**10**	**10**	4.611	5.523	−0.549	1.422	3.179	−3.651	3.231	2.030
TCSC1 Location	–	–	24	13	15	18	12	19	20	20
TCSC2 Location	–	–	16	17	26	14	27	14	25	17
TCSC1 Rating	**0**	**0.5**	0.294	0.480	0.221	0.261	0.437	0.403	0.279	0.204
TCSC2 Rating	**0**	**0.5**	0.213	0.202	0.160	0.243	0.144	0.357	0.322	0.184
TCPS1 Location	–	–	19	16	23	23	28	25	21	20
TCPS2 Location	–	–	22	26	33	23	14	15	31	19
TCPS1 Rating	−**5**	**5**	−1.239	−2.128	−1.398	−0.747	0.304	0.797	−0.187	0.372
TCPS2 Rating	−**5**	**5**	1.618	−0.298	0.373	0.018	0.988	−4.113	1.473	0.005
TFC ($/h)	–	–	**861.489**	**865.902**	**863.797**	**865.736**	**845.768**	**883.242**	**870.299**	**852.611**
Emission (Ton/h)	–	–	**0.166**	**0.164**	**0.165**	**0.163**	–	–	–	–
APL (MW)	–	–	–	–	–	–	**4.010**	**3.024**	**3.458**	**4.066**

Table 14. Multi-objective simulation results for case 9 and case 10.

Control & State Variables	Min	Max	Case-9				Case-10			
			GNDO	**GWO**	**MFO**	**MVO**	**GNDO**	**GWO**	**MFO**	**MVO**
PTG2	**20**	**80**	41.854	40.056	35.406	41.929	52.339	50.960	47.711	57.834
PWG5	**0**	**75**	46.213	44.290	45.659	43.000	73.729	59.378	67.052	72.012
PTG8	**10**	**35**	10.539	17.206	12.905	17.794	27.548	33.079	25.001	34.062
PWG11	**0**	**60**	40.507	37.047	42.067	37.374	55.547	50.930	47.004	45.086
PTG13	**12**	**40**	14.441	14.583	17.107	15.543	25.046	28.260	33.662	29.799
V1	**0.95**	**1.1**	1.095	1.085	1.077	1.077	1.027	1.045	1.039	1.019
V2	**0.95**	**1.1**	1.088	1.068	1.070	1.062	1.026	1.036	1.037	1.030
V5	**0.95**	**1.1**	1.082	1.054	1.052	1.035	1.021	1.024	1.026	1.017
V8	**0.95**	**1.1**	1.089	1.081	1.081	1.078	1.011	1.016	1.009	1.004
V11	**0.95**	**1.1**	1.081	1.067	1.082	1.081	1.042	1.072	1.048	1.033
V13	**0.95**	**1.1**	1.093	1.082	1.078	1.080	1.031	1.010	1.036	1.045
T11	**0.9**	**1.1**	1.022	0.979	0.971	1.001	0.984	1.010	1.032	0.979
T12	**0.9**	**1.1**	0.957	0.945	0.959	1.012	0.963	0.956	0.949	0.929
T15	**0.9**	**1.1**	1.005	1.017	0.979	0.981	0.964	0.964	0.985	0.980
T36	**0.9**	**1.1**	0.909	0.906	0.927	0.910	0.947	0.933	0.943	0.946
SVC1 Location	-	-	17	21	15	21	8	23	22	9
SVC2 Location	-	-	24	14	22	27	19	10	19	19
SVC1 Rating	−**10**	**10**	7.270	1.629	1.395	3.604	0.703	6.496	0.374	−0.378
SVC2 Rating	−**10**	**10**	8.303	3.620	6.583	8.418	6.197	−2.454	6.193	4.988
TCSC1 Location	-	-	38	38	21	15	14	7	11	26
TCSC2 Location	-	-	16	15	38	13	30	24	28	27
TCSC1 Rating	**0**	**0.5**	0.470	0.446	0.273	0.473	0.281	0.097	0.357	0.309
TCSC2 Rating	**0**	**0.5**	0.487	0.410	0.403	0.438	0.186	0.433	0.412	0.384
TCPS1 Location	-	-	30	13	11	14	23	15	25	31
TCPS2 Location	-	-	31	7	14	23	29	14	28	15
TCPS1 Rating	−**5**	**5**	1.527	0.693	0.001	0.286	0.888	1.063	0.635	2.025
TCPS2 Rating	−**5**	**5**	2.980	−0.065	−1.394	−0.272	0.240	2.646	0.126	−0.864
TFC ($/h)	-	-	**810.049**	**814.201**	**813.755**	**817.163**	-	-	-	-
VSI	-	-	**0.105**	**0.110**	**0.116**	**0.115**	-	-	-	-
Total Gross F.C ($/h)	-	-	-	-	-	-	**1173.322**	**1208.416**	**1212.959**	**1199.459**
Voltage Deviation (p.u)	-	-	-	-	-	-	**0.176**	**0.230**	**0.209**	**0.169**

Table 15. Multi-objective simulation results for case 11 and case 12.

Control & State variables	Min	Max	Case-11				Case-12			
			GNDO	GWO	MFO	MVO	GNDO	GWO	MFO	MVO
PTG2	20	80	45.293	44.975	50.298	45.856	31.589	60.147	33.799	36.035
PWG5	0	75	60.666	68.795	62.294	57.155	62.042	61.717	66.094	52.766
PTG8	10	35	24.271	24.485	27.179	26.031	24.651	27.550	25.232	25.207
PWG11	0	60	46.551	47.899	53.206	47.440	40.375	57.220	45.112	41.884
PTG13	12	40	19.146	17.287	20.734	14.419	18.307	15.569	16.090	19.407
V1	0.95	1.1	1.033	1.093	1.060	1.015	1.066	1.046	1.077	1.045
V2	0.95	1.1	1.019	1.086	1.060	1.008	1.058	1.040	1.063	1.032
V5	0.95	1.1	0.997	1.069	1.055	1.001	1.040	0.996	1.041	1.017
V8	0.95	1.1	1.015	1.081	1.051	1.006	1.046	1.039	1.039	1.009
V11	0.95	1.1	1.020	1.040	1.055	1.051	1.051	1.075	1.034	1.037
V13	0.95	1.1	1.035	1.051	1.021	1.019	1.028	1.029	1.052	1.050
T11	0.9	1.1	1.000	0.972	0.999	0.966	0.987	0.963	0.963	0.964
T12	0.9	1.1	1.003	1.070	1.055	1.007	1.020	0.976	1.002	0.973
T15	0.9	1.1	1.061	1.099	1.075	1.043	1.035	1.087	1.051	1.015
T36	0.9	1.1	0.952	1.076	1.024	0.985	0.964	0.974	0.964	0.965
SVC1 Location	-	-	11	21	13	18	14	15	18	18
SVC2 Location	-	-	13	12	15	8	20	23	19	18
SVC1 Rating	−10	10	0.495	6.230	−2.056	−0.109	0.057	3.863	−0.308	−2.293
SVC2 Rating	−10	10	3.861	4.665	5.159	8.132	0.599	3.889	−0.818	7.033
TCSC1 Location	-	-	20	16	21	4	26	39	25	24
TCSC2 Location	-	-	19	24	24	22	17	22	18	23
TCSC1 Rating	0	0.5	0.173	0.269	0.306	0.331	0.217	0.101	0.133	0.278
TCSC2 Rating	0	0.5	0.205	0.288	0.336	0.365	0.312	0.194	0.259	0.237
TCPS1 Location	-	-	15	24	30	8	20	19	17	25
TCPS2 Location	-	-	14	34	20	36	16	20	22	5
TCPS1 Rating	−5	5	0.083	−2.213	1.397	−0.222	0.555	−0.891	0.384	0.657
TCPS2 Rating	−5	5	2.118	−0.241	0.863	0.454	−0.207	−1.208	−0.652	0.936
TFC ($/h)	-	-	868.806	877.252	887.402	860.794	849.334	893.297	860.198	845.253
Emission (Ton/h)	-	-	0.162	0.157	0.150	0.167	-	-	-	-
APL (MW)	-	-	4.034	3.370	3.254	4.347	4.328	3.453	3.922	4.825
VSI	-	-	-	-	-	-	0.416	0.356	0.378	0.269

Table 16. Multi-objective simulation results for case 13.

| Control & State Variables	Min	Max	Case-13			
			GNDO	GWO	MFO	MVO
PTG2	20	80	49.763	52.443	59.634	45.029
PWG5	0	75	47.291	62.622	61.404	53.782
PTG8	10	35	26.717	13.340	15.911	17.846
PWG11	0	60	29.206	58.719	47.380	47.174
PTG13	12	40	26.888	19.443	18.672	18.177
V1	0.95	1.1	1.048	1.034	1.041	1.053
V2	0.95	1.1	1.038	1.012	1.027	1.051
V5	0.95	1.1	1.028	0.980	0.990	1.009
V8	0.95	1.1	1.040	0.998	1.026	1.027
V11	0.95	1.1	1.053	1.069	1.047	1.024
V13	0.95	1.1	1.029	1.054	1.051	1.021
T11	0.9	1.1	1.012	0.931	0.974	0.978
T12	0.9	1.1	0.968	1.046	0.994	1.005
T15	0.9	1.1	1.023	0.975	1.032	1.055
T36	0.9	1.1	0.969	0.943	1.006	0.967
SVC1 Location	-	-	10	15	24	20
SVC2 Location	-	-	18	25	15	20
SVC1 Rating	−10	10	−4.176	6.233	1.560	1.932
SVC2 Rating	−10	10	3.745	6.259	4.766	0.737
TCSC1 Location	-	-	22	6	31	19
TCSC2 Location	-	-	19	27	17	22
TCSC1 Rating	0	0.5	0.423	0.208	0.168	0.228
TCSC2 Rating	0	0.5	0.278	0.300	0.125	0.114
TCPS1 Location	-	-	20	28	27	20
TCPS2 Location	-	-	27	26	32	20
TCPS1 Rating	−5	5	−0.164	−3.317	−0.896	−0.585
TCPS2 Rating	−5	5	1.413	−2.786	−0.976	0.658
TFC ($/h)			863.417	883.480	874.361	850.096
Emission (Ton/h)			0.173	0.157	0.160	0.175
APL (MW)			5.189	4.628	4.265	4.809
Voltage Deviation (p.u)			0.359	0.225	0.450	0.529
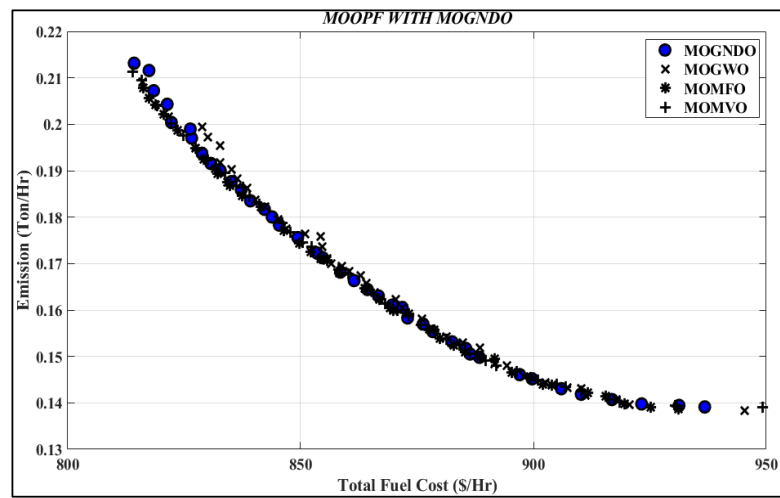
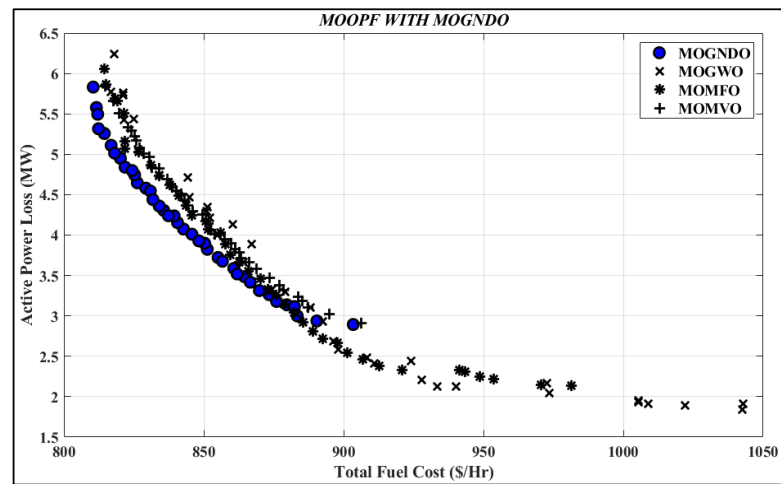**Figure 20.** PF of TFC and emission minimization.
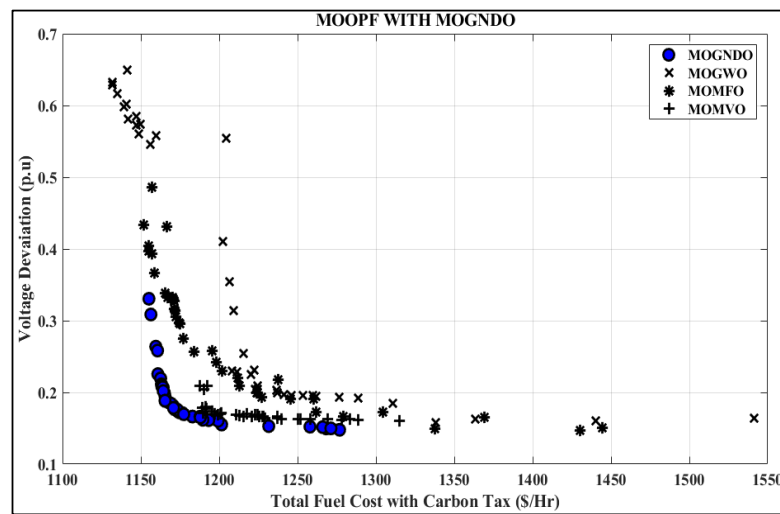

Figure 21. PF of TFC and APL minimization.

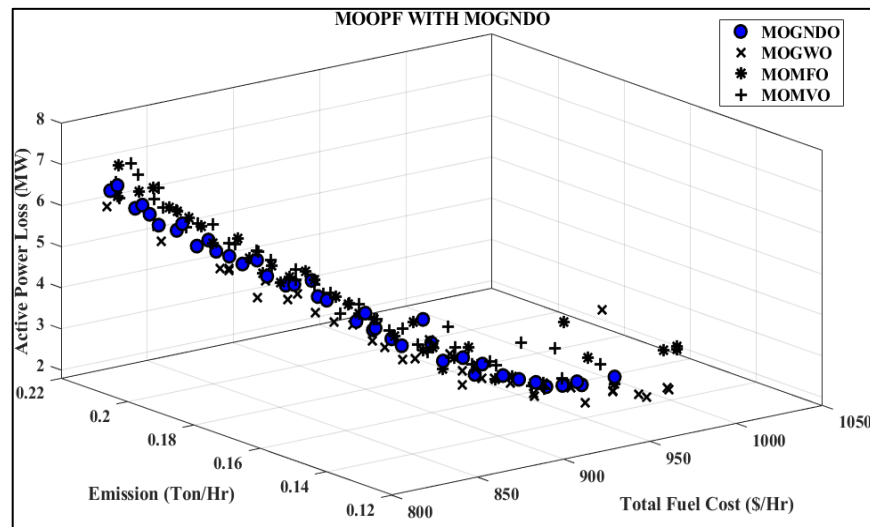**Figure 22.** PF of TFC with a carbon tax and voltage deviation minimization.

Figure 23. PF of TFC, emission, and APL minimization with different algorithms.
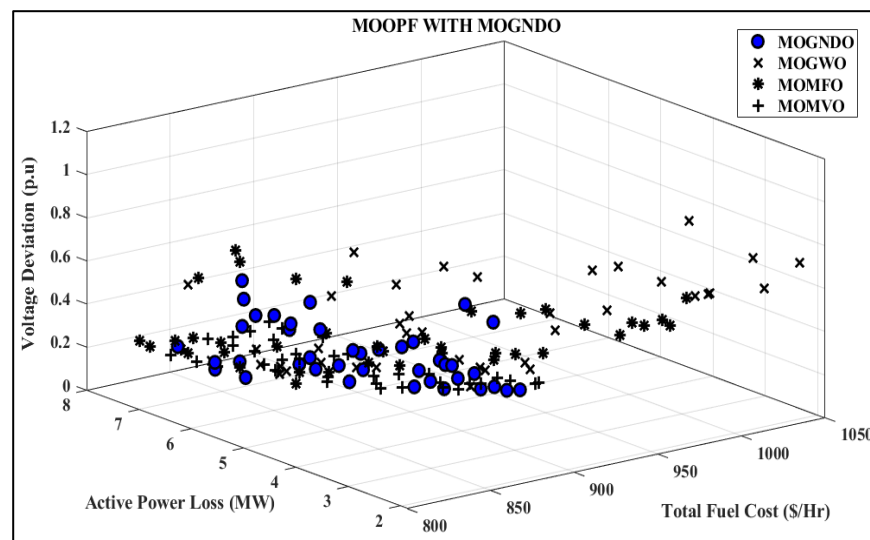

Figure 24. PF of TFC, APL, and voltage deviation minimization with different algorithms.

The MOGNDO methodology was one of the finest methods for finding the best solutions to the multi-objective OPF problem that integrated with wind power plants and the appropriate placement of FACTS devices, according to the tabulated data.

6. Conclusions

The optimal location and size of FACTS devices in this study, as well as single- and multi-objective optimal power flow (MOOPF) concerned coal-based and wind power plants, which were all addressed by the solution technique. Different probability density functions were used to express inconsistencies in unconventional resource availability. The method for integrating each unit was described in detail. When utilizing non-conventional sources of energy sources and FACTS devices, single objectives were optimized, such as generation cost, toxic gas emanation, voltage deviation, active loss, and VSI. A multi-objective form of the OPF problem was looked into in light of the current situation of the electric network. The outcomes were contrasted with a recently created optimization strategy. Based on the results, it can be said that the proposed MOGNDO outperformed existing algorithms in terms of convergence, and delivered higher quality and more usable

solutions for each situation involving optimal power flow. All of the results point to the suggested technique's significant advantage in obtaining the best solutions to OPF issues with one or more objectives. Finally, it was shown that by integrating wind farms with FACTS devices utilizing a non-dominated sorting technique, MOGNDO could be successfully employed to address small and large optimal power flow challenges. Based on the extensive analysis of the proposed MOGNDO, the following can be summarized as its advantages—

- Randomization in MOGNDO includes the diversity of the Pareto front being enhanced, since all solutions in the first dominated front will have an equal chance of being selected, and multi-objectives are made uniformly significant while performing local exploration.
- MOGNDO can deal with large-scale search spaces and is less dependent on problem characteristics. Moreover, these algorithms are capable of estimating multiple points in the search domain simultaneously, due to their population-based nature.
- MOGNDO strikes a good balance between exploitation and exploration, providing powerful searchability for finding the optimum solution
- MOGNDO is superior in terms of the balance of diversity and convergence, the distribution of PF, and better convergence.

Author Contributions: Conceptualization, S.B.P., J.V. and M.M.; Methodology, S.B.P., J.V., M.M. and T.K.M.; Software, T.K.M. and P.J.; Validation, S.B.P., M.M. and T.K.M.; Formal analysis, J.V., M.M. and T.K.M.; Investigation, S.B.P.; Resources, P.J.; Data curation, J.V. and P.J.; Writing—original draft, S.B.P., J.V., M.M., T.K.M. and P.J.; Writing—review & editing, S.B.P.; Visualization, T.K.M. and P.J.; Supervision, S.B.P.; Funding acquisition, M.M. All authors have read and agreed to the published version of the manuscript.

Institutional Review Board Statement: Not applicable.

Informed Consent Statement: Not applicable.

Data Availability Statement: The data presented in this study are available in the article.

Conflicts of Interest: The authors declare no conflict of interest.

Abbreviations

Acronyms

OPF	Optimal Power Flow
Mas	Meta Heuristics Algorithms
MOGNDO	Multi-Objective Generalized Normal Distribution Optimization
TG	Thermal Generating unit
WG	Wind Generation
ISO	Independent System Operator
PDF	Probability Density Function
BCS	Best Compromise Solution
MOMFO	Multi-Objective Moth Flame Optimization
MOOPF	Multi-Objective Optimal Power Flow
SHADE-SF	Success History-based Adaptive Differential Evolution using Superiority of Feasible solutions method
DE-SF	Differential Evolution using Superiority of Feasible solutions method
ABC-SF	Artificial Bee Colony using Superiority of Feasible solutions method
PSO-SF	Particle Swarm Optimization using Superiority of Feasible solutions method

FPA-SF	Flower Pollination Algorithm using Superiority of Feasible solutions method
MSA-SF	Moth Swarm Algorithm using Superiority of Feasible solutions method
TFC	Total Fuel Cost
APL	Active power Loss
VSI	Voltage Stability Index

Nomenclature

a_i, b_i, c_i, e_i and d_i	Price constants for ith coal-based power plants.
α_i, β_i, γ_i, ω_i and μ_i	Toxic gas emanation constants concerning the ith coal-based units.
g_w	Direct cost constant
P_{ws}	Scheduled power of the wind unit.
K_{Rw}	Reserve cost coefficient regarding wind unit
K_{Pw}	Penalty cost coefficient of wind unit
P_{ws}	Accessible power from the wind unit
P_{wr}	Specified output power from the wind unit
$f_w(p_w)$	Wind energy probability density function for the wind unit.
v_{in}, v_r and v_{out}	Cut-in, rated, and cut-out wind velocity of the turbine respectively
p_{wr}	Rated value of the generated output of the wind turbine
τ	Degree of series compensation
X_{mn}	Line inductive reactance linking buses m and n
R_{mn}	Resistance of the line linking buses m and n
V_m and V_n	Bus voltage magnitudes linking buses m and n.
δ_m and δ_n	Phase angles of the linking buses m and n
g_{mn} and b_{mn}	Conductance and susceptance of the line linking buses m and n.
N_{pq}	Number of load (PQ) buses
v_i	pu voltage level of ith bus.
P_{Gi} and P_{Di}	Generation and dispatch at ith bus
	Number of buses
Y_1 and Y_2	Sub-matrices of
$\delta_{ij} = \delta_i - \delta_j$	Variance in phase angles of voltage among bus i and bus
P_{Di} and Q_{Di}	Real and VAR power demand respectively at ith bus
P_{Gi} and Q_{Gi}	Real and VAR outputs respectively of ith bus by either unit (coal-based or non-conventional) as applicable
G_{ij} and B_{ij}	Conductance and susceptance between bus i and bus j

References

1. Joshi, M.; Ghadai, R.K.; Madhu, S.; Kalita, K.; Gao, X.-Z. Comparison of NSGA-II, MOALO and MODA for Multi-Objective Optimization of Micro-Machining Processes. *Materials* **2021**, *14*, 5109. [CrossRef] [PubMed]
2. Cao, B.; Li, M.; Liu, X.; Zhao, J.; Cao, W.; Lv, Z. Many-objective deployment optimization for a drone-assisted camera network. *IEEE Trans. Netw. Sci. Eng.* **2021**, *8*, 2756–2764. [CrossRef]
3. Liang, X.; Luo, L.; Hu, S.; Li, Y. Mapping the knowledge frontiers and evolution of decision making based on agent-based modeling. *Knowl.-Based Syst.* **2022**, *250*, 108982. [CrossRef]
4. Zhang, K.; Wang, Z.; Chen, G.; Zhang, L.; Yang, Y.; Yao, C.; Wang, J.; Yao, J. Training effective deep reinforcement learning agents for real-time life-cycle production optimization. *J. Pet. Sci. Eng.* **2022**, *208*, 109766. [CrossRef]
5. Ganesh, N.; Ghadai, R.K.; Bhoi, A.K.; Kalita, K.; Gao, X.-Z. An intelligent predictive model-based multi-response optimization of EDM process. *Comput. Model. Eng. Sci.* **2020**, *124*, 459–476. [CrossRef]
6. Ghadai, R.K.; Kalita, K.; Gao, X.-Z. Symbolic regression metamodel based multi-response optimization of EDM process. *FME Trans.* **2020**, *48*, 404–410. [CrossRef]
7. Cao, B.; Zhang, W.; Wang, X.; Zhao, J.; Gu, Y.; Zhang, Y. A memetic algorithm based on two_Arch2 for multi-depot heterogeneous-vehicle capacitated arc routing problem. *Swarm Evol. Comput.* **2021**, *63*, 100864. [CrossRef]
8. Liu, Y.; Zhang, Z.; Liu, X.; Wang, L.; Xia, X. Ore image classification based on small deep learning model: Evaluation and optimization of model depth, model structure and data size. *Miner. Eng.* **2021**, *172*, 107020. [CrossRef]
9. Ullah, Z.; Wang, S.; Radosavljevic, J.; Lai, J. A solution to the optimal power flow problem considering WT and PV generation. *IEEE Access* **2019**, *7*, 46763–46772. [CrossRef]
10. Elattar, E.E. Optimal power flow of a power system incorporating stochastic wind power based on modified moth swarm algorithm. *IEEE Access* **2019**, *7*, 89581–89593. [CrossRef]

11. Man-Im, A.; Ongsakul, W.; Singh, J.G.; Madhu, M.N. Multi-objective optimal power flow considering wind power cost functions using enhanced PSO with chaotic mutation and stochastic weights. *Electr. Eng.* **2019**, *101*, 699–718. [CrossRef]

12. Salkuti, S.R. Optimal power flow using multi-objective glowworm swarm optimization algorithm in a wind energy integrated power system. *Int. J. Green Energy* **2019**, *16*, 1547–1561. [CrossRef]

13. Kathiravan, R.; Kumudini Devi, R.P. Optimal power flow model incorporating wind, solar, and bundled solar-thermal power in the restructured Indian power system. *Int. J. Green Energy* **2017**, *14*, 934–950. [CrossRef]

14. Duman, S.; Rivera, S.; Li, J.; Wu, L. Optimal power flow of power systems with controllable wind-photovoltaic energy systems via differential evolutionary particle swarm optimization. *Int. Trans. Electr. Energy Syst.* **2020**, *30*. [CrossRef]

15. Duman, S.; Li, J.; Wu, L.; Guvenc, U. Optimal power flow with stochastic wind power and FACTS devices: A modified hybrid PSOGSA with chaotic maps approach. *Neural Comput. Appl.* **2020**, *32*, 8463–8492. [CrossRef]

16. Biswas, P.P.; Suganthan, P.N.; Qu, B.Y.; Amaratunga, G.A.J. Multiobjective economic-environmental power dispatch with stochastic wind-solar-small hydro power. *Energy* **2018**, *150*, 1039–1057. [CrossRef]

17. Chen, M.-R.; Zeng, G.-Q.; Lu, K.-D. Constrained multi-objective population extremal optimization based economic-emission dispatch incorporating renewable energy resources. *Renew. Energy* **2019**, *143*, 277–294. [CrossRef]

18. Chang, Y.-C.; Lee, T.-Y.; Chen, C.-L.; Jan, R.-M. Optimal power flow of a wind-thermal generation system. *Int. J. Electr. Power Energy Syst.* **2014**, *55*, 312–320. [CrossRef]

19. Saha, A.; Bhattacharya, A.; Das, P.; Chakraborty, A.K. A novel approach towards uncertainty modeling in multiobjective optimal power flow with renewable integration. *Int. Trans. Electr. Energy Syst.* **2019**, *29*. [CrossRef]

20. Biswas, P.P.; Suganthan, P.N.; Amaratunga, G.A.J. Optimal power flow solutions incorporating stochastic wind and solar power. *Energy Convers. Manag.* **2017**, *148*, 1194–1207. [CrossRef]

21. Ben Hmida, J.; Chambers, T.; Lee, J. Solving constrained optimal power flow with renewables using hybrid modified imperialist competitive algorithm and sequential quadratic programming. *Electr. Power Syst. Res.* **2019**, *177*, 105989. [CrossRef]

22. Pandya, S.; Jariwala, H.R. Single- and multiobjective optimal power flow with stochastic wind and solar power plants using moth flame optimization algorithm. *Smart Sci.* **2022**, *10*, 77–117. [CrossRef]

23. Biswas, P.P.; Arora, P.; Mallipeddi, R.; Suganthan, P.N.; Panigrahi, B.K. Optimal placement and sizing of FACTS devices for optimal power flow in a wind power integrated electrical network. *Neural Comput. Appl.* **2021**, *33*, 6753–6774. [CrossRef]

24. Wolpert, D.H.; Macready, W.G. No free lunch theorems for optimization. *IEEE Trans. Evol. Comput.* **1997**, *1*, 67–82. [CrossRef]

25. Zhang, Y.; Jin, Z.; Mirjalili, S. Generalized normal distribution optimization and its applications in parameter extraction of photovoltaic models. *Energy Convers. Manag.* **2020**, *224*, 113301. [CrossRef]

26. Kumar, S.; Jangir, P.; Tejani, G.G.; Premkumar, M.; Alhelou, H.H. MOPGO: A new physics-based multi-objective plasma generation optimizer for solving structural optimization problems. *IEEE Access* **2021**, *9*, 84982–85016. [CrossRef]

27. Mirjalili, S. SCA: A Sine Cosine Algorithm for solving optimization problems. *Knowl. Based Syst.* **2016**, *96*, 120–133. [CrossRef]

28. Mirjalili, S. The ant lion optimizer. *Adv. Eng. Softw.* **2015**, *83*, 80–98. [CrossRef]

29. Javidy, B.; Hatamlou, A.; Mirjalili, S. Ions motion algorithm for solving optimization problems. *Appl. Soft Comput.* **2015**, *32*, 72–79. [CrossRef]